Icarus 426 (2025) 116349

Contents lists available at ScienceDirect

Icarus

journal homepage: www.elsevier.com/locate/icarus

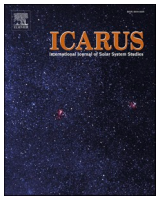

A modeling approach for water and sediment transport in Jezero crater on Mars based on new geomorphological evidence

Anastasiia Ovchinnikova *, Ralf Jaumann, Sebastian H.G. Walter, Christoph Gross, Wilhelm Zuschneid, Frank Postberg

Institute for Geological Sciences, Freie Universität Berlin, Malteserstr. 74-100 / Buildings A, B, C, D, E, N, T, 12249 Berlin, Germany

ARTICLE INFO

Keywords:
Mars, surface
Mars, climate
Geological processes
Impact processes

ABSTRACT

In our study we examined water-related processes and events in the Jezero crater on Mars using flow discharge and sediment transport models of: 1) the western inlet valley carving, 2) the northern inlet valley carving, 3) crater flooding by only northern inlet and 4) by both northern and western inlets, 5) erosion of the western rim by the western inlet, 6) erosion of the eastern rim due to the outlet, 7) water outflow from the crater, 8) outlet valley carving, 9) western delta deposition, 10) northern delta deposition. Detailed geomorphological analyses, delta and valley mapping and measurements served as a base for our investigations. As our knowledge is limited mostly to remote sensing data and only few in situ data from the Perseverance rover, a range of scenarios for each event was modeled by varying, where necessary, the values of input parameters – grain size, channel depth, channel width, channel slope, median grain size, 90th percentile grain size. We calculated the minimum time-scales and the minimum volume of available water for each event. The obtained results were interpreted, taking into account the limitations of the model. We found that: 1) the northern inlet participated in the first crater flooding and the eastern rim breaching and it alone could have flooded the crater; 2) the northern and western deltas were deposited during the last incisions of the corresponding inlets; 3) Jezero crater was flooded multiple times, implying open-basin lake conditions during or after the eastern rim breaching. Our findings complement results and interpretations of previous studies and also reveal new insights into the fluvial history in Jezero crater.

1. Introduction

Jezero crater – the investigation site of the current NASA's Mars 2020 mission – has been actively studied for almost 20 years. Since it was first described in detail in [Fassett and Head, 2005], it was believed to once have contained a lake. Not only the geomorphological evidence – two inlets, entering the crater from the west and the north, the outlet valley, exiting the crater to the east and two delta deposits in the west and north accordingly to inlets – support this idea, but also the detection of clay minerals (first – from orbital data [Poulet et al., 2005], [Bibring et al., 2006], [Mangold et al., 2007], [Murchie et al., 2009]), which form under the presence of water. These arguments in favor of a paleolake in Jezero led to its selection as the target landing site for Mars 2020, one of the goals of which is to search for signs of possible ancient life. As at least episodic access to liquid water is almost universally accepted to be necessary for life (e.g. [Mottl et al., 2007]; [Jaumann et al., 2014]), constraining the fluvial activity in Jezero can contribute to its habitability assessment.

Jezero crater (diameter ~ 50 km) is located at the highland/lowland boundary on Mars [Tanaka et al., 2014] between the Nili Fossae region to the northwest, Isidis Planitia to the east and Syrtis Major to the southwest. The Nili Fossae region (Middle Noachian age, [Tanaka et al., 2014]) is dominated by large grabens concentric to the Isidis impact basin, the grabens are considered to be the tectonic response to the basin formation ([Comer et al., 1985], [Wichman and Schultz, 1989], [Goudge et al., 2015]). Isidis Planitia, which was formed in the Noachian as a result of an impact, was later resurfaced by volcanic and fluvial/glacial activities in the Late Noachian – Early Amazonian and by wind activity since the early Amazonian [Ivanov et al., 2012]. The Syrtis Major volcanic province has Early Hesperian age [Hiesinger and Head, 2004]. The Jezero crater itself is interpreted to be formed in the Noachian period: younger than the Isidis impact basin (~3.85–4.05 Ga

* Corresponding author.
E-mail address: a.ovchinnikova@fu-berlin.de (A. Ovchinnikova).

https://doi.org/10.1016/j.icarus.2024.116349
Received 2 July 2024; Received in revised form 27 September 2024; Accepted 15 October 2024
Available online 19 October 2024

[Robbins et al., 2013]) and older than the first fluvial activity within the crater (based on the crater counts on the valleys of the Jezero, the fluvial system is estimated to be of ~3.8 Ga [Fassett and Head, 2008], [Goudge et al., 2015]). The fluvial activity in the crater is constrained to the Noachian-Hesperian boundary, based on crater counting of the valleys [Fassett and Head, 2008] and the western delta [Mangold et al., 2020].

Recent spectroscopic and geologic in situ observations by the Perseverance rover found igneous rocks altered by water [Farley et al., 2022], [Corpolongo et al., 2023], [Rice et al., 2023] and even detected specific fluorescence-mineral associations consistent with many classes of organic molecules [Sharma et al., 2023]. These findings support the idea that Jezero was a paleolake in the past. Several researchers tried to reconstruct, at least partly, the history of the paleolake using different approaches: 1) geomorphological analysis of the crater and valley discharge estimations [Fassett and Head, 2005], 2) analysis of the clay-rich fluvial–lacustrine sediments of THEMIS and CRISM data [Ehlmann et al., 2008], 3) analysis of the scroll bars and epsilon cross-bedding on the delta [Schon et al., 2012], 4) a quantitative geomorphological study of the inlet valleys [Mangold et al., 2020], 5) modeling of the five water-related events (western valley carving, crater flooding by the western inlet, the eastern rim erosion, water outflow during the breaching and western delta deposition) [Salese et al., 2020], 6) photogeologic mapping ([Stack et al., 2020], [Jodhpurkar et al., 2024]), 7) study of the stratigraphic relations between the main western delta deposit, isolated mesas and crater floor units [Holm-Alwmark et al., 2021], 8) images of the delta outcrop taken by Perseverance [Mangold et al., 2021], 9) hydrological models to constrain the climatic and hydrological conditions in Jezero [Horvath and Andrews-Hanna, 2024] and 10) topographic detrending techniques to accentuate topographic features of the volcanic floor to study possible old locations of lakes and rivers in Jezero [Annex and Ehlmann, 2024]. Moreover, several attempts were undertaken to model the outlet formation of Jezero – [Fassett and Goudge, 2017], [Holo and Kite, 2017], [Fassett and Goudge, 2021].

In our research we were inspired by the study of [Salese et al., 2020] and modeled all (ten) possible water-related processes using sediment and water transport models developed by [Kleinhans, 2005]. Moreover, we took into account the new data from the Perseverance rover [Stack et al., 2024], as well as careful measurements and our geomorphological observations based on the latest available remote sensing data to get more plausible input data to the model. The modeled events (processes) included: 1) western inlet (Neretva Vallis) valley carving, 2) northern inlet (Sava Vallis) valley carving, 3) crater flooding by only northern inlet and 4) by both northern and western inlets, 5) western rim breaching, 6) eastern rim breaching 7) water outflow from the crater, 8) outlet valley (Pliva Vallis) carving, 9) western delta deposition, 10) northern delta deposition (Fig. 1). Under "valley carving" we mean erosion of the valleys by flowing water; under "rim breaching" – erosion of the rim by ponding water, which overflows the edge of the rim. The goal of our study was to calculate the minimum timescales for each event and estimate the minimum volume of water provided/released during each event. The modeling results together with geomorphological observations allowed us to draw new conclusions about water activity in the crater and answer the questions: 1) which inlets were involved in the crater flooding; 2) when in the relative chronology of the crater's fluvial activity the northern and western deltas were deposited; and 3) whether there was enough water to flood the crater repeatedly and maintain open lake conditions for a long time.

Our study started with the definition of the model, mapping deltas and valleys, their morphometric measurements, as well as crater volume and diameter determination, and eastern rim breach and western rim breach volumes measurements (Section 2. Methods; Section 3.1. Results of measurements). The geomorphological analysis (Section 3.2. Geomorphological observations) added new information, which had to be taken into account during modeling. For example, we identified 2 incision events of the valleys; showed the importance of including the northern inlet to the model (which was not done in previous researches);

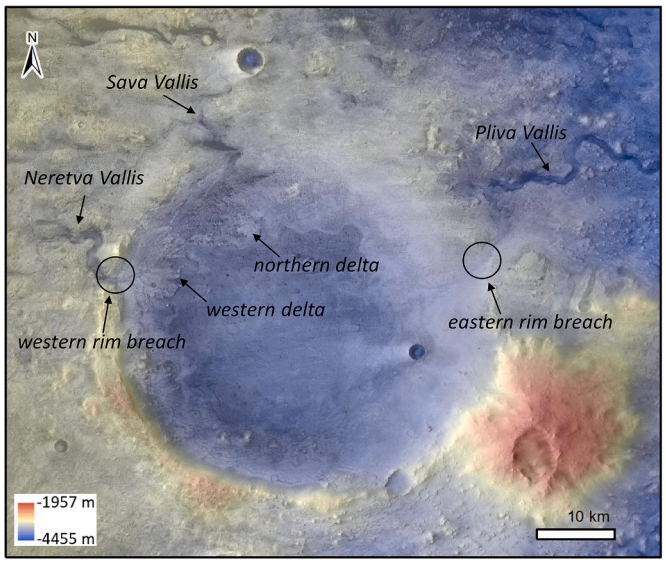

Fig. 1. Jezero's main features, studied in this paper (HRSC Mars Chart (HMC_13E10) DTM (50 m/pixel), overlayed by corresponding ortho-rectified image mosaics).

for the first time we also analyzed the western rim breach to include it in the model. After that we modeled ten water-related events, applying a variety of input parameters to study a range of possible scenarios (Section 3.3. Results of modeling). We checked the uncertainties of results (coming from the uncertainties of the data, methods and the model itself) to set limits for our interpretation (Section 4.1. Understanding of the obtained results). After that we interpreted the obtained timescales (Section 4.2. Relative comparison of timescales) and minimum available of water for each event (Section 4.3. Calculation of the minimum available water amount). We also considered the "fresh unfilled crater" case and showed that increasing the crater volume will not influence our interpretations (Section 4.4. Discussion, "Missing Sediments and the Fresh Crater Case"). Finally, we compared our interpretation with previous studies in Section 4.4. Discussion, "Comparison With Previous Studies". Based on these studies, we achieved a better understanding on how the water-related (water transport and sediment transport) processes and events in the Jezero crater were interconnected, how they influenced each other and how they overlapped with each other.

2. Methods

2.1. Model description

We use flow discharge and sediment transport models for Martian conditions developed by Kleinhans [Kleinhans, 2005] which have been already applied many times to hydrological systems of Mars (for example, [Jaumann et al., 2010], [Hoke et al., 2011], [Mangold et al., 2012], [Adeli et al., 2016]). Goal of the Kleinhans' models is to calculate water and sediment transport timescales under constant bank-full discharge. These are the conditions when most of the erosion occurs, because bank-full discharge can be assumed as the channel forming discharge for fluvial channels [Leopold et al., 1964]). Bank-full conditions are conditions when water fills the whole channel to its banks but does not overtop them; discharge then is maximum [Leopold et al., 1964]). Studies on the frequency of bank-full discharges on Earth show different cycles for different regions – from half a year for many English rivers to 10 years in Pennsylvania [Harvey, 1969]; a recent study for the United States shows a 1.5-year cycle, although there are substantial variations around this numbers [Simon et al., 2004]. Another estimation is that channel-forming discharges on Earth occur for about 5 % of the fluvial active time [Parker, 2005]. For Mars there are only some

estimates on the intermittency factor for fluvial activity: for the Paraná Valles region near the Noachian–Hesperian boundary it yields ~0.01–0.1 % during 10^5–10^6 yr (Buhler et al., 2014). However, the question of the periodicity of the bank-full cycles on Mars as well as the longevity and periodicity of lake activity (Michalski et al., 2022) remains outstanding.

It is important to note that climate is not the only factor which determines bank-full conditions – river cross-section, channel slope, porosity of the substrate, grain size of the sediment and other geological and climatological factors also play a role [Kleinhans, 2005]. For example, the type of the water source (ground-water sapping/precipitation/snow melting/etc.) determines the response to intensive precipitation. As shown by [Laity and Malin, 1985; Howard et al., 1988; Dunne, 1990], reaction of the sapping channel networks to precipitation is slower than that of the overland flow networks. Therefore, it is reasonable to assume that in this situation, a river fed by groundwater sapping would have a longer cycle of bank-full conditions than a precipitation-fed river. Moreover, river cross-section and channel slope also influence the bank-full cycle duration: it tends to increase as the river slope increases [Chau et al., 2021].

The Kleinhans models are based on water and sediment balances. For the water transport events they answer the question how long it takes for a certain amount of water to flow through a given channel (in bank-full conditions) and for the sediment transport events they can be used to compute how long it takes to transport a certain amount of sediment through a given channel (in bank-full conditions). Therefore, timescales are calculated by dividing the transported amount of the water by the water discharge and by dividing the transported amount of the sediment by the sediment transport rate. Climate conditions are not involved in the model; single water events could be separated by long durations. Therefore, timescales obtained here are minimum values. For example, deltas could have formed by the multiple episodes of water flow and sediment deposition. In our study we generalize the episodes of delta formation and consider the entire period of delta formation as a single delta-forming event in order to get an estimate of quantitative parameters.

A detailed description of the model is written in Kleinhans, 2005. The formulas have been rewritten to show our step-by-step calculation approach (the desired parameter is always on the left side of the equation).

For the water transport timescale calculation, the channel size (width w, depth h, slope s), the volume of the transported water V_w and the median grain size D_{50} should be measured or estimated. Martian gravity g is known and taken as 3.72 m/s^2. First, the hydraulic radius R_h and the friction factor f (after Eq. 13 in Kleinhans, 2005) should be calculated in order to estimate the friction of the channel floor and walls on the flow:

$$R_h = \frac{w \cdot h}{w + 2h} \tag{1}$$

$$f = \frac{8}{\left(2.2 \cdot \left(\frac{h}{D_{50}}\right)^{-0.055} \cdot s^{-0.275}\right)^2} \tag{2}$$

Second, the Darcy-Weisbach equation [Silberman et al., 1963] is used to calculate the depth- and width-averaged flow velocity:

$$u = \sqrt{\frac{8 \cdot g \cdot R_h \cdot s}{f}} \tag{3}$$

Third, channel width and depths together with flow velocity allow to calculate water discharge:

$$Q_w = w \cdot h \cdot u \tag{4}$$

Finally, the timescale of the water transport event is obtained by dividing the transported water volume by the discharge:

$$T_w = \frac{V_w}{Q_w} \tag{5}$$

Sediments can be transported as bed load (along the stream bed by rolling or sliding) or as suspended load (which is uplifted in the flow) and it is possible to model both transport modes. ***To calculate the timescale of sediment transport under suspended load conditions***, channel sizes (w, h, s), the volume of the transported sediment (V_s), median grain size (D_{50}), the sediment density ρ_s and the porosity λ should be measured or estimated. The Martian gravity g (3.72 m/s^2) and the fluid density ρ_w (for water – 1000 kg/m^3) are known. First, the friction factor f is obtained using Eq. (2). Second, the relative submerged density – a dimensionless measure of sediments buoyancy – is calculated:

$$R = \frac{\rho_s - \rho_w}{\rho_w} \tag{6}$$

The third step is the calculation of the bed shear stress (Eq. (7)), which acts on the sediments covering the bed and initiates their motion. Following Kleinhans, 2005, it is derived as the force of a block of water of unit length and width, with the water depth h over the channel bed and the slope s. In that case it is called the total shear stress of the flow because it is related to the total friction of the channel and includes both the bedform-related shear stress and grain-related shear stress. The nondimensionalized bed shear stress – the Shields parameter (Eq. (8)) – is calculated then from the bed shear stress:

$$\tau_{total} = \rho_w \cdot g \cdot h \cdot \sin s \tag{7}$$

$$\theta = \frac{\tau}{(\rho_s - \rho_w) \cdot g \cdot D_{50}} \tag{8}$$

The non-dimensional total transport rate (Eq. (9)) is taken as sediment transport predictor, which was postulated by Engelund and Hansen, 1967 and used in Kleinhans, 2010. Subsequently, the Specific Volumetric Transport Rate (Eq. (10)) is calculated, which describes sediment transport per unit width per unit time (m^3 per m width per second) and accounts for the pore space λ. After that, the Volumetric Transport Rate (Eq. (11)) can be obtained by multiplying by the channel width:

$$\phi_s = \frac{0.1}{f} \theta^{2.5} \tag{9}$$

$$Q_{s\_spec} = \left(\frac{1}{1-\lambda}\right) \cdot \phi_s \cdot \sqrt{R \cdot g} \cdot D_{50}^{\frac{3}{2}} \tag{10}$$

$$Q_s = Q_{s\_spec} \cdot w \tag{11}$$

Finally, the timescale of sediment transport assuming suspended load (Eq. (12)) is calculated by dividing the volume of the transported sediment V_s by the volumetric transport rate:

$$T_s = \frac{V_s}{Q_s} \tag{12}$$

To calculate sediment transport timescale under bed load conditions, the friction factor, the relative submerged density, the hydraulic radius and the velocity are calculated according to formulas (2), (6), (1), (3). Then, the 90th percentile grain size D_{90} (and skin friction) can be calculated following the empirical relation, which was used in Salese, 2020:

$$D_{90} = 5 \cdot D_{50} \tag{13}$$

Next, the grain friction factor (Eq. (14)) is taken as roughness predictor from the White-Colebrook function [Silberman et al., 1963] (see Eq. 8 in Kleinhans, 2005); the value D90 is chosen as hydraulic roughness length k_s (following Kleinhans, 2005). The grain shear stress (Eq. (15)) is then calculated to represent the shear force on the grains which

is needed for the computation of the near-bed sediment transport (Eq. 17 in Kleinhans, 2005):

$$f_{gr} = \frac{8}{\left(5.74 \cdot log\left(12.2 \cdot \frac{R}{D_{90}}\right)\right)^2} \quad (14)$$

$$\tau_{gr} = \frac{1}{8} \cdot \rho_w \cdot f_{gr} \cdot u^2 \quad (15)$$

After that the grain-related non-dimensionalized grain shear stress – the grain-related Shields parameter (Eq. (16)) – is calculated (eq. 22 in Kleinhans, 2005). It is needed to obtain the non-dimensional total transport rate (eq.17), which is also called the Meyer-Peter and Mueller predictor [Meyer-Peter and Mueller, 1948], [Kleinhans and van Rijn, 2002]. Here the Shields criterion for incipient motion (θ_{cr}) is included (eq. 30 in Kleinhans, 2005), which could be calculated using different empirical relations (see Section "4.3. Predictive Bed State Criteria and Diagram" in Kleinhans, 2005). Here we use $\theta_{cr} = 0.03$ as in Kleinhans, 2010:

$$\theta_{gr} = \frac{\tau_{gr}}{(\rho_s - \rho_w) \cdot g \cdot D_{50}} \quad (16)$$

$$\phi_b = 8 \cdot (\theta_{gr} - \theta_{cr})^{1.5} \quad (17)$$

Last steps include the specific volumetric transport rate (Eq. (18)), the volumetric transport rate (Eq. (19)), and the timescale of sediment transport assuming bed load (Eq. (20)):

$$Q_{b\_spec} = \left(\frac{1}{1-\lambda}\right) \cdot \phi_b \cdot \sqrt{R \cdot g} \cdot D_{50}^{\frac{3}{2}} \quad (18)$$

$$Q_b = Q_{b\_spec} \cdot w \quad (19)$$

$$T_b = \frac{V_b}{Q_b} \quad (20)$$

To decide which transport mode (suspended load or bed load) is more probable, the suspended/bed load transport ratio ("S/B ratio") is used: if it is far larger than one, then the system is suspension-dominated [Kleinhans, 2005; Salese et al., 2020]. Kleinhans et al., 2010 decide to use five as a threshold. In our study we followed this approach as it also gives the widest possible range of timescales than using a threshold equal to one.

2.2. Methods of measurements

We use the Mars 2020 Science Investigation CTX DEM Mosaic (20 m/pixel) and corresponding ortho-mosaic (5 m/pixel) for mapping the deltas and for subsequent volume measurements ([[dataset] Calef, 2021], [Malin et al., 2007]); valley mapping and volume measurements were based on the HRSC Mars Chart (HMC_13E10) DTM (50 m/pixel) and the related ortho-rectified image mosaics (12.5 m/pixel) [Gwinner et al., 2016]. The HRSC Mars Chart (HMC) data was accessed via the map-based data portal at https://maps.planet.fu-berlin.de (Walter et al., 2018) and converted to the IAU (International Astronomical Union) system with a sphere radius of 3,396,190 m. For the channel measurements we use both the Mars 2020 Science Investigation CTX DEM and Ortho-Mosaics and the Mars 2020 Terrain Relative Navigation HiRISE DTM Mosaic (1 m/pixel) with the corresponding Ortho-Mosaics (0.25 m/pixel) ([Fergason et al., 2020], [Malin et al., 2007]). The data were co-registered to HRSC and reprojected to a sinusoidal projection.

Before measuring, the deltas and the valleys were mapped at a scale of 1:5000. The valleys were mapped using two morphological features (Fig.SM1–5, Supplementary Material). We assume that they represent two distinct phases in valley development and are not expressions of different lithologies. The first is the initial old valley, which has no borders that are recognizable in image data. It was mapped based on slope and curvature rasters derived from the HRSC DTM. The second is the last incised valley, which was mapped on the HMC ortho-rectified image mosaic. The difference between the borders can be seen in Fig. 2, Fig. 3 and Fig. SM1–5 (Supplementary Material). In the upper section of the western inlet (starting from the valley head, to about 130 km to the east) it appears that the initial valley is broader than the last incised valley, whereas in the lower section (the easternmost 70 km) the visible borders of the initial and the last incised valleys almost coincide (Fig. 3). This is explained by the fact that the lower section is covered by an olivine-bearing unit [Mangold et al., 2020]. It blanketed the lower part of the initial valley and the interior and the rim of the Jezero crater [Mangold et al., 2020; Goudge et al., 2015]). As a result, any former fluvial and lacustrine deposits within this area were also buried by this unit. The lower section of the last incised valley was carved into the olivine-bearing unit after its emplacement. Therefore, the volume of the initial valley is underestimated in its lower section. Where the boundaries of the initial valley were not traceable in the Slope raster, we have drawn them in the same way as the valley boundaries of the last incision (based on the HMC mosaic).

To map the last incised valleys of inlets and outlet, first, certain and uncertain borders of the valleys were identified on the HMC ortho-mosaics as well as the flow traces. However, the borders of the northern valley are not continuous, therefore they were approximated in the most realistic way using information of the slope gradient direction derived from the HMC DTM (Fig. 4).

As a result, all three valleys – western (Neretva Vallis), northern (Sava Vallis) and outlet (Pliva Vallis) were mapped in 2 extents – initial valley and last incised valley extents (Fig. SM1–5, Supplementary Material).

Both deltas were mapped with 3 possible extents: minimum, medium and maximum (Fig. 5 and Fig. 6). The minimum extent for the western delta is based on the GIS version of the map of [Stack et al., 2020]. Delta map units "blocky", "layered rough", "thickly layered", "thinly layered", "truncated curvilinear layered" were merged into one single polygon for the purpose of this study. For the medium extent the western borders remain the same while the eastern borders were set according to the nearest buttes. The maximum extent includes controversial areas to the north and to the west (near the crater rim) while in the south and in the east the extent is following the farthest buttes.

Mapping the extent of the northern delta is more challenging, because it is heavily eroded. For the minimum extent we followed the steep edge (although sometimes it is destroyed and only remnants are left) in the west and in the south (without buttes). In the east we followed the border from the map of Jodhpurkar et al., 2024 and Jodhpurkar and Bell, 2024, who mapped two geological units based on a change of surface properties along this border. The medium extent in general follows the borders of the minimum extent, but in the south the closest buttes are included. The maximum extent includes controversial areas in the west (closer to the eroded crater rim), in the north the border starts at the valley entrance to the crater, in the east we followed the borders from the map of Goudge et al., 2013, and in the south the most distal buttes were included.

Measurements were conducted in ArcGIS. Width, depth, and slope of the channels were measured using longitudinal and cross-sectional profiles on the CTX DTM. Salese et al., 2020 observed a 5 m-high terrace within the western valley at the entrance into the Jezero crater (see Fig. 2 in their paper) and used it as a bank-full channel depth of the western inlet. Following this methodology, we also found a channel terrace in the northern valley (with the average depth 4.6 m) and a channel terrace in the outlet valley (with the average depth 13 m) (see Fig. SM8–9, Supplementary Material); these values were taken as channel depths in the model. The water volume needed to fill the crater before breaching was determined as the crater volume up to the elevation of the first breaching terrace (recognized at the eastern rim where the outlet is exiting the crater – see Fig. 8 and Section 3.2. Geomorphological observations) using the standard Surface Volume Tool. It

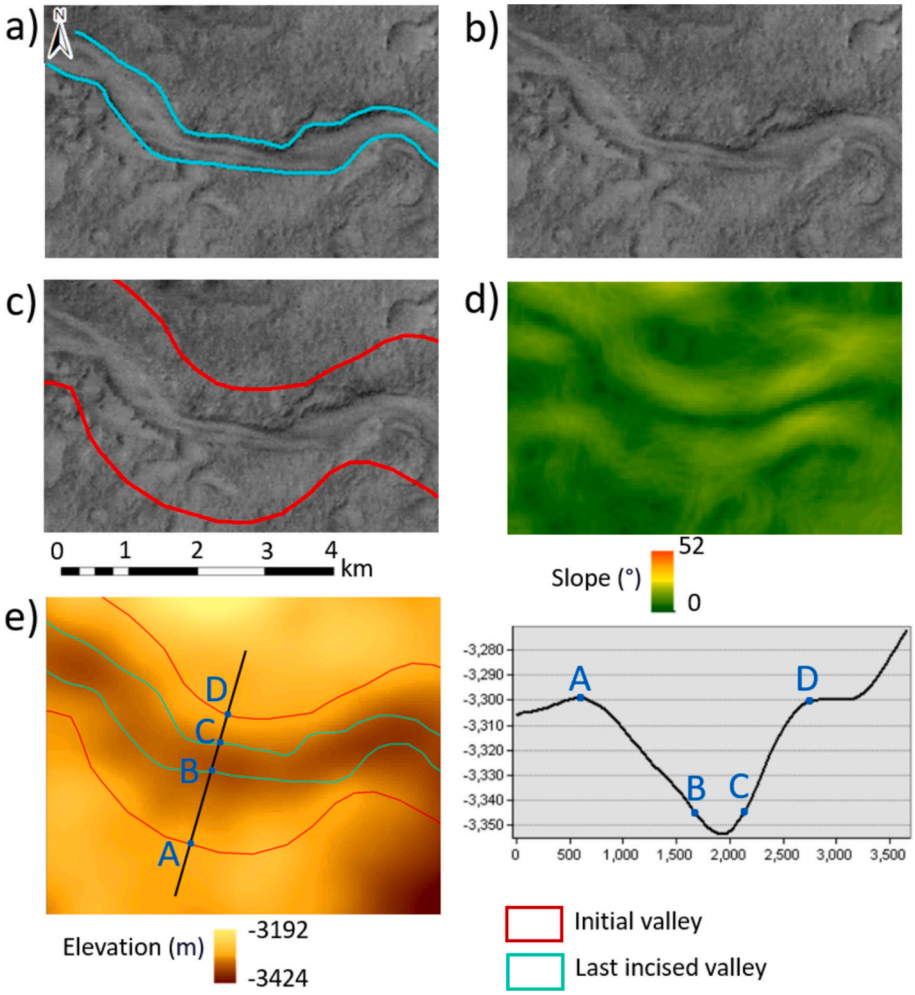

Fig. 2. Segments of the last incised western valley (a), mapped on the HMC ortho-mosaic (b) and the initial valley (c), mapped on slope raster (d) and profile curvature raster, calculated from the HMC DTM. e) – Elevation profile through the initial valley and last incised valley (on HMC DTM) which shows that the boundaries of the initial valley are located at the convex bends of the valley profile (points A and D). Therefore, they are drawn along the area between the steep slope (yellow color) and a flat surface (green color) – Fig. 2c and d. (For interpretation of the references to color in this figure legend, the reader is referred to the web version of this article.)

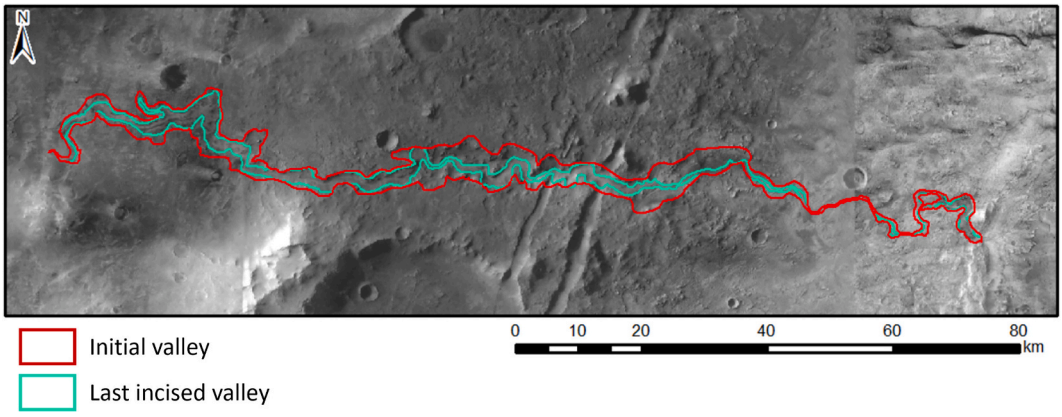

Fig. 3. Initial western valley (mapped on slope and profile curvature rasters, calculated from the HMC DTM) and the last incised western valley (mapped on the HMC ortho-mosaic).

calculates the volume between the DTM and the horizontal plane of a certain elevation (in this case −2243 m). Similarly, the minimum volume of water that outflowed during the eastern rim breaching was estimated. This amount of water was stored between the level of the 1st breaching terrace and the outlet floor at the eastern rim. The third type of measurements is the volume of the eroded and deposited sediments. The eroded volume of the western rim breach and the eastern rim breach (not only the total volume, but also the volumes eroded during each

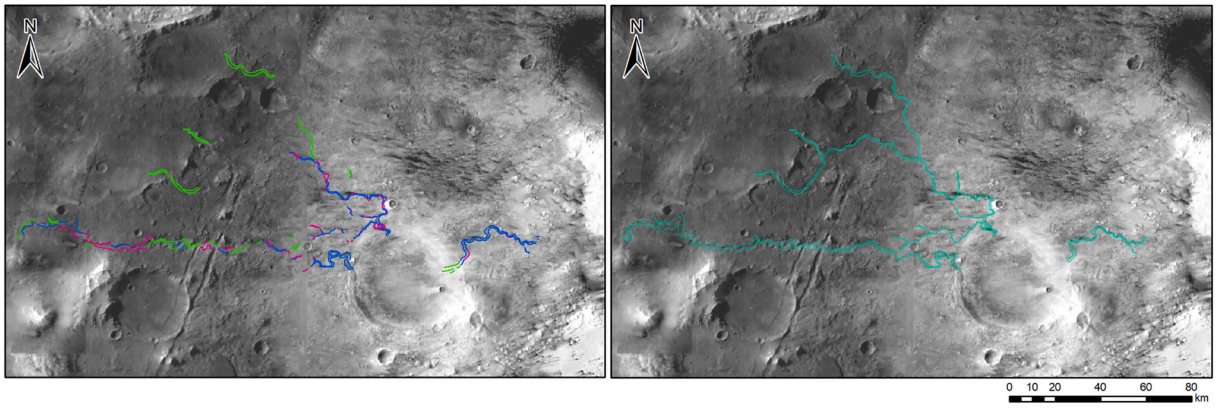

Fig. 4. Approximation of the mapped borders of the last incised valleys in the most realistic way.

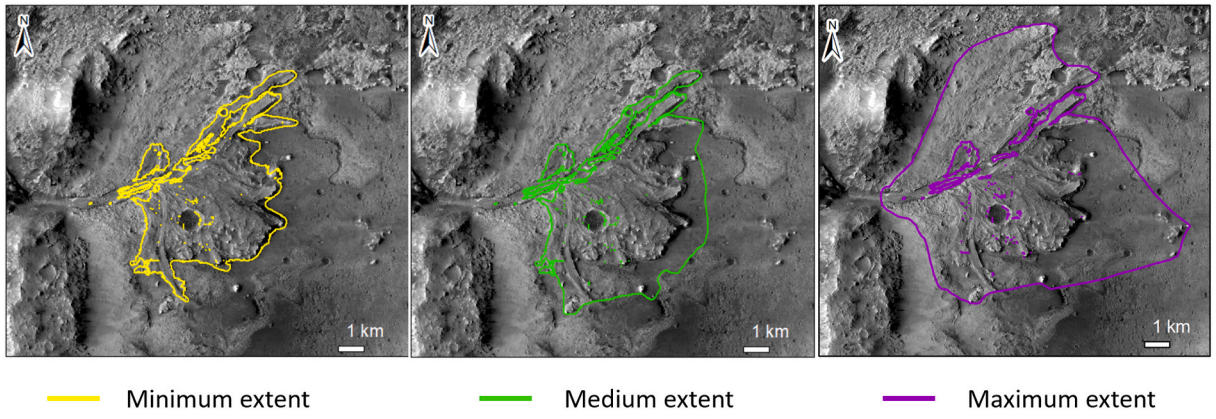

Fig. 5. Western delta in 3 extents (description of borders in the text).

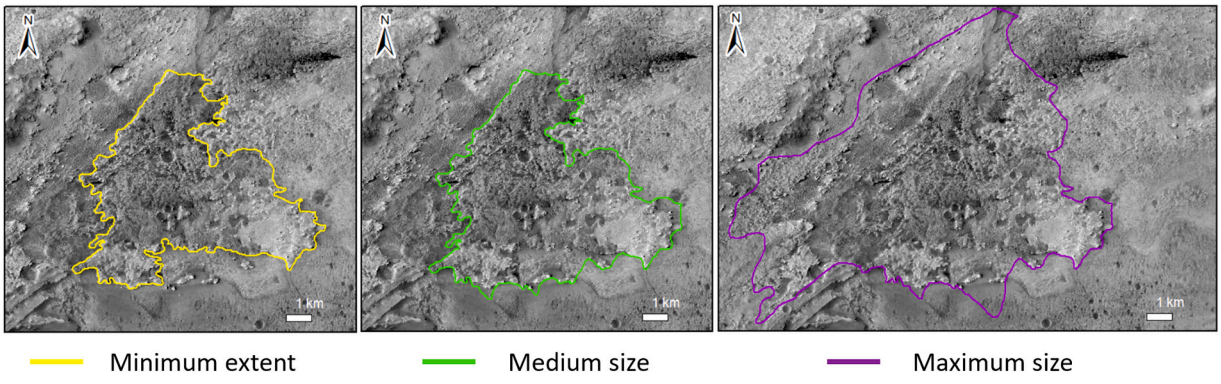

Fig. 6. Northern delta in 3 extents (description of borders in the text).

breaching phase) was estimated using the Surface Volume Tool and information about the elevations of each breaching terrace. Our method accounts not only for the changing distances between terraces for each breaching phase, but also for the narrowing of the rim ridge upward.

To measure volumes of the valleys, the mapped borders were transformed into a sequence of points with an interval of 50 m using the "Generate Points Along Lines" tool in ArcGIS. To each point the height information was added from the DTM using the "Add Surface Information" tool. After that, the "Natural Neighbor" tool was used to interpolate the surface which existed before the valley carving. Finally, the obtained surface was overlapped with the actual DTM of the valley in the "CutFill tool" to calculate the volume of the eroded rock. To cross-check the results of this method, we roughly estimated the volume by multiplying the valley area by its mean depth. The results were in good agreement.

For estimating the volumes of the deltas two methods were used: 1)

minimum, medium and maximum volumes were calculated by multiplying the delta area by the mean delta thickness (40 m for the northern and 60 m for the western delta, measured on cross-section profiles); 2) the actual delta volume was measured using the CTX DTM. For this, a tilted plane was created using information about the delta slope (assuming that the surface under the delta has the same slope as the delta itself) – Fig. 7. This plane, lowered by the mean delta thickness (60 m), represents the underlying surface. Overlapping with the actual DTM in the "CutFill tool" gives the volume of the deposited sediments.

The measurement uncertainties were also assessed. The first measurement uncertainty arises from distortions associated with the map projection. To assess this uncertainty, we followed the methods of Butcher et al., 2016 and Butcher et al., 2020 by comparing the lengths of 1° meridional lines in different places over the study area, measured in planar and geodetic mode. The differences were minor (~1 %).

The uncertainty of the vertical measurements and thus the volume measurements directly depend on the internal vertical error of the DEM or DTM, which means the same thing on Mars. For the Mars 2020 Science Investigation CTX DEM Mosaic, which is used for most of the measurements with exception of valley lengths and volumes, the intrinsic (relative) vertical error originating from merging of the several stereo combinations into the final DTM mosaic is described separately for the western part and for the eastern part of the mosaic. The western part of Mosaic has relative vertical offsets of 3.8 m between the individual CTX DEMs [Fergason et al., 2020]; for the eastern part only an approximate qualitative assessment is available – vertical offsets are not greater than ~10 m here (dataset author Fred Calef, personal communication, February 6, 2024). For the HRSC Mars Chart DTM the overall internal consistency of the data can be described by the mean intersection error which summarizes the precision of all object points [Gwinner et al., 2009]. For example, for the MC-11 quadrangle subset the mean intersection error for all points in multi-orbit DEM is not more than 8.9 m [Gwinner et al., 2016]. Approximately the same error is expected for the MC-13 quadrangle subset which was used in this study. The Mars 2020 Terrain Relative Navigation HiRISE DTM Mosaic has a median vertical offset to the CTX DTM mosaic of the Lander Vision System elevation map equal to ~0.4 m.

The uncertainties due to the human factor and manual digitalization of the features by the choice of exact points to draw the borders of objects are usually insignificant in morphometric studies and do not exceed 1 % [Butcher et al., 2016].

3. Results

3.1. Results of measurements

The measured key parameters are shown in Table 1. They can be classified into three groups: 1) characteristics of the channels – width, depth, slope – to calculate discharge and sediment transport rate; 2) volume of the crater – to estimate water volume needed to fill the crater before the eastern rim breaching; 3) delta volumes, valley volumes and carved rim volumes – to estimate the amount of transported/deposited sediments. The obtained values are consistent with those obtained in previous studies ([Stack et al., 2020], [Salese et al., 2020], [Mangold et al., 2020], [Mangold et al., 2021], [Gazetteer of Planetary Nomenclature, International Astronomical Union (IAU), 2024], [Ehlmann et al., 2008], [Schon et al., 2012]). This shows that the developed measurement methods are reliable and that the values obtained for features which were not studied before are plausible (northern inlet measurements, western rim breach, outlet measurements).

The western delta and the western valley are larger than correspondingly the northern delta and the northern valley. The amount of material eroded from the valleys during the last incision (8 km^3 for the western valley and 2 km^3 for the northern) is approximately the same as deposited in deltas (1.44–4.58 km^3 for the western delta and 1.58–3.73 km^3 for the northern). That means that, with high probability, the deltas were deposited during the last incision of the valleys. Goudge et al., 2018 reported about the incision on top of the western delta which they mapped as Jezero Western Delta (JWD) valley (see Fig. 2 in their paper). This would imply that the last cutting phase was after the delta was deposited. However, this does not contradict our observations and interpretations, because JWD valley (width 500–600 m, depth 30–50 m – see Fig. 7 in Goudge et al., 2018) is smaller than our mapped western last incised valley (mean width ~ 1200 m, depth ~ 140 m) and one valley can be nested in another. Moreover, channel which was carved during the last cutting phase after the delta was deposited (Fig. 2 in Goudge et al., 2018) would have smaller size within the last incised valley mapped in our study, as there it would cut the more competent bedrock to the west of the crater rim in contrast to less competent alluvial material within the delta itself. The deposition of the transported sediments from the initial valleys will be discussed in Section 4.4. Discussion. The lengths of the main tributaries of the western and northern valleys are comparable – 210 km and 160 km, accordingly. However, the western inlet (~3000 m width and ~ 200 m depth) is significantly more incised than the northern inlet (~2000 m width and ~ 100 m). This shows that the western inlet was formed by more extensive erosion, hinting at a longer period of fluvial activity. It is worth mentioning that valleys today might be mantled with aeolian deposits and mass wasting material

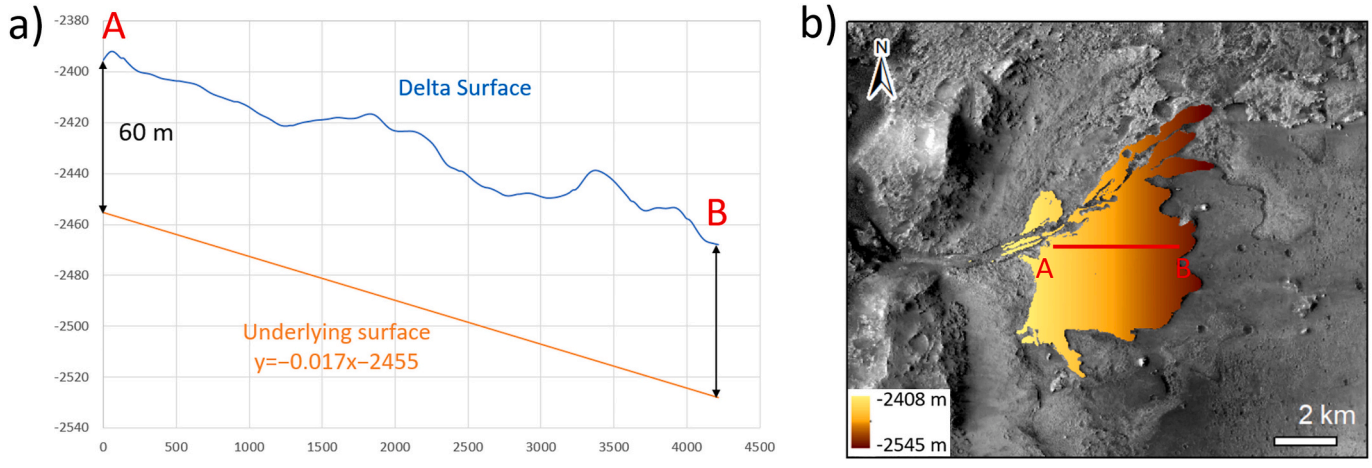

Fig. 7. a) Profiles of the delta surface and obtained underlying surface; b) Plan view of the underlying surface.

Table 1
Morphometry of the Jezero crater. * For the "tilted plane method" explanation see Section 2.2. Methods of measurements. References in the table: Gazetteer of Planetary Nomenclature, International Astronomical Union (IAU)(2024), Ehlmann et al. (2008), Fassett and Head (2005), Goudge et al. (2015); Mangold et al. (2020), Mangold et al. (2021), Salese et al. (2020), Schon et al. (2012), Stack et al. (2020).

Measured feature		In this study	In previous studies
Diameter of the crater		50 km	50 km [Stack et al., 2020], [Salese et al., 2020] 45 km [Mangold et al., 2021] 47.52 km [Gazetteer of Planetary Nomenclature, International Astronomical Union (IAU), 2024]
Crater volume below −2243 m (to flood the crater before breaching)		446 km^3	463 km^3 [Salese et al., 2020]
Western inlet	Length of the main tributary	210 km	~200 km [Mangold et al., 2020]
	Total valley volume (including last incised valley)	42 km^3	56 km^3 [Mangold et al., 2020] 58 km^3 [Ehlmann et al., 2008]
	Last incised valley volume	8 km^3	
	Initial valley volume (without last incised valley)	34 km^3	
	Mean width of the last incised valley	~1200 m	4 km – maximum width [Mangold et al., 2020]
	Mean width of the initial valley	~3000 m	
	Mean depth of the last incised valley	~140 m	400 m – maximum depth; <<50 m – minimum [Mangold et al., 2020]
	Mean depth of the initial valley	~200 m	
	Mean channel width	190 m	190 m [Salese et al., 2020], 200–500 m [Mangold et al., 2020]
	Mean channel depth	5 m	5 m [Salese et al., 2020], [Mangold et al., 2020]
	Channel slope	0.0095	0.0097 [Salese et al., 2020], 0.007–0.017 [Mangold et al., 2020]
Northern inlet	Length of the main tributary	60 km	> 80 km [Mangold et al., 2020]
	Total valley volume (including last incised valley)	9.5 km^3	–
	Last incised valley volume	2 km^3	
	Initial valley volume (without last Incised valley)	7.5 km^3	
	Mean width of the last incised valley	~700 m	–
	Mean width of the initial valley	~2000 m	
	Mean depth of the last incised valley	~50 m	–
	Mean depth of the initial valley	~100 m	
	Mean channel width	196 m	–
	Mean channel depth	4.6 m	–
	Channel slope	0.013248	–
Outlet	Length of the outlet	60 km	~53 km [Schon et al., 2012] > 70 km [Mangold et al., 2020]
	Total valley volume (including last incised valley)	4 km^3	12 km^3 [Salese et al., 2020]
	Last incised valley volume	1 km^3	
	Initial valley volume (without last incised valley)	4–1 = 3 km^3	
	Mean width of the last incised valley	~1000 m	–
	Mean width of the initial valley	~2000 m	
	Mean depth of the last incised valley	~100 m	–
	Mean depth of the initial valley	~200 m	
	Mean channel width	400 m	–
	Mean channel depth	13 m	–
	Channel slope	0.012516	–
Western Delta	Minimum extent (measured on DTM)	1.07 km^3	5 km^3 ([Fassett and Head, 2005]; [Ehlmann et al., 2008]); 7.8 km^3 [Goudge et al., 2015]; 5–15 km^3 [Salese et al., 2020]
	Minimum extent ("tilted plane" method*)	1.44 km^3	
	Medium extent	2.06 km^3	
	Maximum extent	4.58 km^3	
Northern Delta	Minimum extent (measured on DTM)	1 km^3	–
	Minimum extent ("tilted plane" method*)	1.58 km^3	
	Medium extent	1.78 km^3	
	Maximum extent	3.73 km^3	
Western Rim Breach	Breach volume	1 km^3	–
	Maximum width of the breach channel	1844 m	–
	Maximum depth of the breach channel	257 m	–
Eastern Rim Breach	Total breach volume	3.1 km^3	3 km^3 [Salese et al., 2020]
	1st breach volume	0.9 km^3	
	2nd breach volume	0.6 km^3	
	3rd breach volume	1.6 km^3	

(continued on next page)

Table 1 (*continued*)

Measured feature			In this study	In previous studies
	Maximum width of the breach channel	1st breach	7550 m	5208 m Salese et al., 2020
		2nd breach	5240 m	3962 m Salese et al., 2020
		3rd breach	3400 m	2114 m Salese et al., 2020
	Maximum depth of the breach channel	1st breach	37 m	37 m Salese et al., 2020
		2nd breach	30 m	28 m Salese et al., 2020
		3rd breach	100 m	98 m Salese et al., 2020
Volume of water outflow during eastern rim breaching (stored between levels of the 1st breaching terrace and outlet floor at the eastern rim)	Total		236 km^3	238 km^3 Salese et al., 2020
	1st breach		56 km^3	57 km^3 Salese et al., 2020
	2nd breach		44 km^3	44 km^3 Salese et al., 2020
	3rd breach		136 km^3	137 km^3 Salese et al., 2020

and were deeper in the past; therefore, depths of valleys and channels and their volumes obtained in this study are minimum values.

In the outlet also an initial valley and a last incised valley were found (Fig. SM5, Supplementary Material), which could be interpreted as 2 erosion events or 2 phases of erosion within the outlet formation. The distinctly visible part of its length is shorter (60 km) than the inlet valleys, however, taking into account sudden interruption of the valley due to possible post-formational erosion of its downstream part, it could be longer (>80 km) and flow directly to the dichotomy border which is located nearby (to the east). Another possibility is that the flow could spread out into different directions. There is at least one bifurcated channel, which is visible in CTX imagery. Therefore, there could also be more channels, smaller and shallower, continuously branching into more streams, creating a sheetwash towards the lowlands at the dichotomy boundary. The third possible reason for the sudden valley disappearance may have been the infiltration of the water into a highly porous rock or underground drainage systems with sinkholes and caves, although this explanation is speculative since there are no sink hole detections in the vicinity of Jezero so far. Finally, the channel erosion could be limited due to transition to deposition which happened in the presence of the hypothetical standing body of water in the Isidis basin.

Concerning channel metrics, we found that mean channel depths and widths in the western inlet and the northern inlet are almost the same (for the western – ~190 m width and ~ 5 m depth; for the northern – ~196 m width and ~ 5 m depth). However, the channel slope is steeper for the northern inlet channel (~0.0132) than for the western (~0.0095), resulting in higher velocity for nearly the same cross-section assuming bank-full flow. This in turn implies higher discharge. In the outlet the mean channel depth (~13 m) and width (~400 m) are greater than in both inlets, while the slope (~0.0125) is comparable to the northern inlet.

We also determined the volumes of the western and eastern rim breaches. The amount of carved rim material is 1 km^3 and 3.1 km^3, respectively. We did not conduct measurements for the northern rim breach because we assumed that the entire northern segment of the rim was already eroded by the time of fluvial activity and had approximately the same morphology which we see now. It could be eroded by the ancient aeolian activity or, for example, by possible coastal abrasion when Jezero was submerged under Arabia ocean (Baum et al., 2021). This assumption is plausible and confirmed by our results (see Section 4.3. Calculation of the minimum available water amount). In addition, the absence of the northern segment of the rim makes the reconstruction of the northern rim breach impossible.

The diameter of the crater, the crater volume below −2243 m (the flood stage before eastern rim breaching) and the minimum volume of water outflow during breaching were re-measured and agree with the values obtained by previous researchers (see Table 1).

3.2. Geomorphological observations

3.2.1. Terraces in the inlets and outlet

In [Salese et al., 2020] it was shown that there are 3 breaching terraces at elevations −2243 m, −2280 m and − 2310 m at the outlet rim which allowed them to hypothesize 3 different phases within the breaching event (Fig. 2R in [Salese et al., 2020]). We also analyzed a profile along the eastern rim and found these breaching terraces (Fig. 8) to be in agreement with Salese's hypothesis.

Our geomorphological analysis of the northern inlet reveals terraces at approximately the same height as the terraces at the eastern rim (Fig. 9). The elevation difference between recognized terraces in the northern inlet and terraces at the eastern rim does not exceed 10 m, which lies in between the vertical errors of the DTM (measurement uncertainties are discussed in Section 2.2. Methods of measurements). These observations indicate that the northern inlet was active during the eastern rim breaching and, therefore, was involved in the flooding phase which later led to the creation of the outlet at the eastern rim. Another point is that these terraces lie outside the last incised valley, indicating that they were formed before the last incision event. The terraces on the right river bank (to the west from the northern inlet) are apparently accumulative, while terraces on the left river bank (to the east from the northern inlet) are due to an erosive origin – as indicated by the valley bend on this site.

The western inlet, in contrast, has no terraces at the breaching levels of the eastern (outlet) rim (−2243 m, −2280 m and −2310 m). This means that it either did not participate in crater flooding, or its terraces were eroded, or that the water flow at the time of the eastern rim breaching was above these levels. Later (in Section 4.3. Calculation of the minimum available water amount) we show that, even if the western inlet was involved in the first crater flooding, the western rim was more likely not carved down to these levels (−2243 m, −2280 m and −2310 m) at the time of the eastern rim breaching.

However, the western rim exposes one distinct terrace at the elevation −2085 m and two small terrace fragments (or morphologic steps) of uncertain origin at the elevations −1800 m and −1990 m (Fig. 10). According to topography to the west from the crater, during breaching of the western rim the water could not rise above the level of approximately −2085 m, because otherwise it would overflow the river banks and flow to the south and to the north around the crater. In this case it would be impossible for water to pond in front of the western rim and breach it. Therefore, we modeled the western rim breaching as one phase breaching between levels of −2342 m and −2085 m.

3.2.2. Western and northern deltas

Both deltas lie below the −2360 m isoline (Fig. SM7, Supplementary Material). Assuming that they were not much higher before they were eroded, this indicates that they were formed when the water level in the lake was <−2360 m. Deposition therefore started during the last breaching phase (which happened between the 3rd eastern rim terrace at a level of −2310 m and the outlet floor at the eastern rim at a level of −2410 m). A similar conclusion was published in [Salese et al., 2020] for the western delta. However, on the DTM in this paper the western delta lies below −2410 m, suggesting delta deposition occurred after

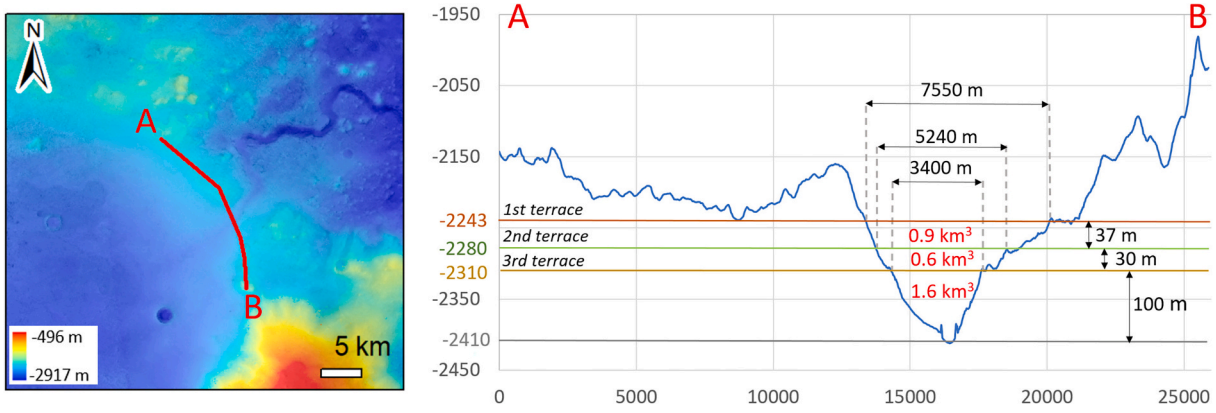

Fig. 8. Profile through the eastern rim showing the three breaching terraces, the maximum width and depth of the breached channels and the volume of material eroded (in red) during each breaching phase. (For interpretation of the references to color in this figure legend, the reader is referred to the web version of this article.)

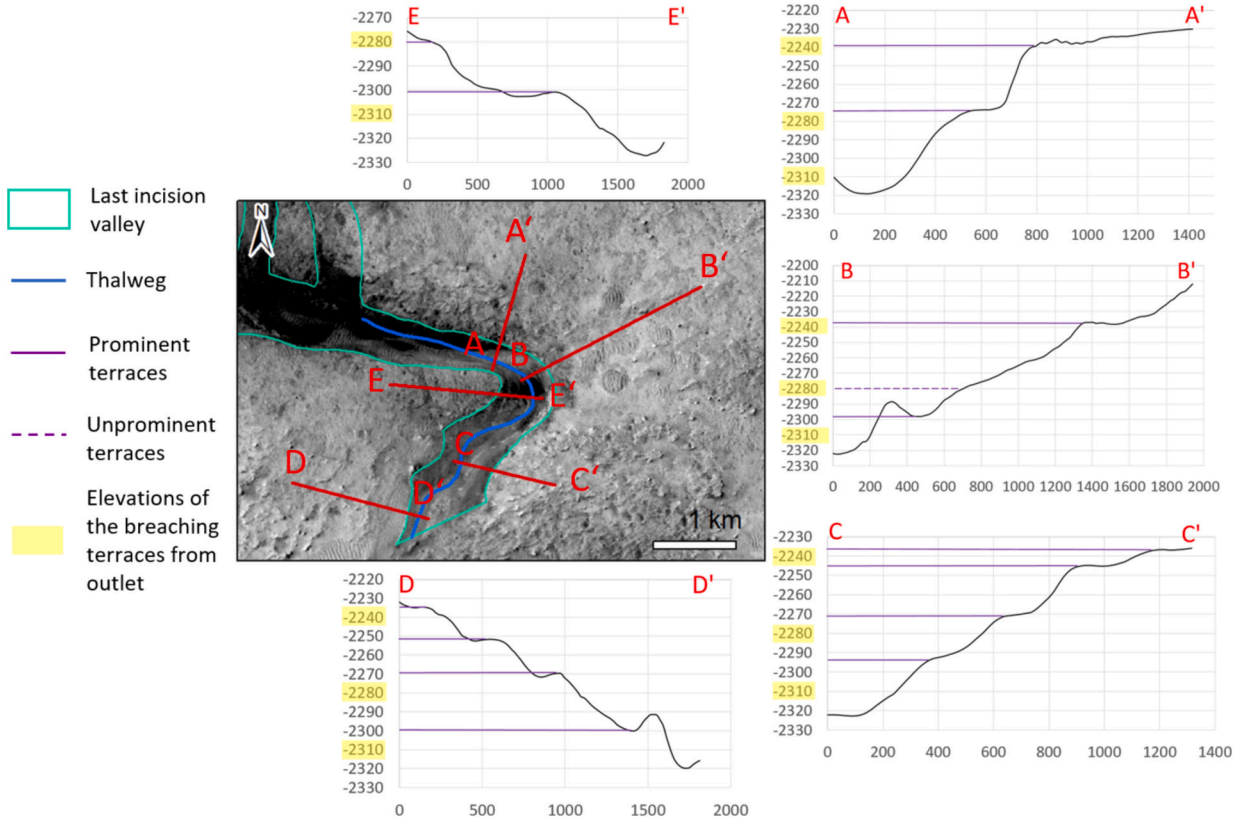

Fig. 9. Terraces at the northern inlet lie approximately at the same heights as the breaching terraces at the eastern rim, indicating that the northern inlet was active during the eastern rim breaching, therefore, also participated in the crater flooding before breaching.

eastern rim erosion, water outflow and subsequent lake level decrease to approximately −2410 m (the height of the outlet floor at the eastern rim). Nevertheless, it is just a small difference compared to our measurements. The main result from our observation is that carving of the last incised valleys coincided with the deposition of the deltas, and these 2 events happened not earlier than during the last breaching phase. These findings are in agreement with Mangold et al., 2024, who found out that delta deposition occurred during a rapid decrease of the water level.

We do not exclude the possibility of the existence of a paleo-delta in the past, which might have been later covered and eroded. This would explain the fate of the 43 km^3 eroded from initial valleys (see also Section 4.4. Discussion).

3.3. Results of modeling

The obtained timescales of water-related events are presented in Table 2. The modeling results in detail for each water-related event can be found in the Supplementary Material (Tables SM1–14).

For modeling, the Martian gravity was taken as 3.72 m/s^2, water density as 1000 kg/m^3, sediment density as 3500 kg/m^3 as assumed for Martian basaltic rock by Kleinhans, 2005 and Salese et al., 2020, sediment porosity as 0.2 as assumed by Kleinhans et al., 2010 and Salese et al., 2020, and Shields criterion for incipient motion as 0.03 as in Kleinhans, 2005 and Salese et al., 2020. The recent study by Beyssac et al., 2024 showed that the olivine-rich boulders in the upper fan and margin unit at Jezero crater are olivine cumulates, which texture and

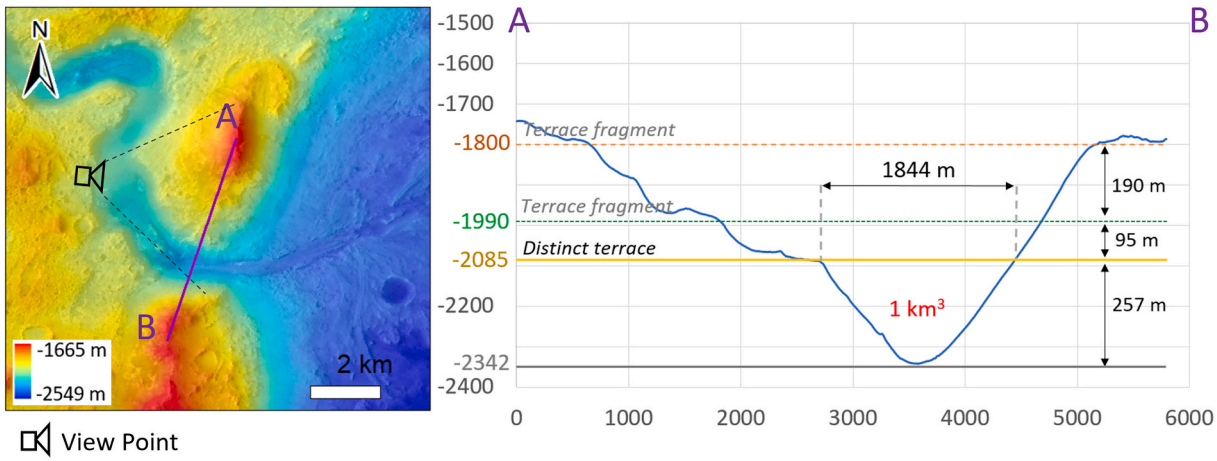

Fig. 10. Distinct terrace at the elevation −2085 m and two small terrace fragments of uncertain origin at the elevations −1800 m and –1990 m. Breaching was modeled up to terrace at −2085 m (see explanation in text). "View Point" is placed to show the perspective view (Fig. SM6, Supplementary Material).

composition align with those of terrestrial dunite. Dunite is a high-density rock (dunite density in Martian meteorite is 3460 kg/m^3 – Coulson et al., 2007) which is consistent with the value of sediment density assumed in this study.

3.3.1. *Valley carving and delta deposition*

The timescales for eroding the northern valley, the western valley and the outlet valley were calculated for both the initial valley volume and last incised valley volume. To assess the timescales of the initial valley incisions, we used the same discharge as calculated for the channel measured within the last incised valley, assuming discharge was approximately similar during both incision periods. In Section 4.4. Discussion we show that even decreasing and increasing the dimensions of the initial valley channel by a factor of 2 will not influence our final interpretation.

We modeled a range of scenarios of Median Grain Size (D50) for the valley carving and delta deposition. Following Salese et al., 2020, we assume the more alluvial environment for Jezero's western and northern inlets, therefore we used D50 from 0.005 m to 0.014 m, which correspond to pebble. The timescales for the intermediate D50 values – 0.008 m, 0.01 m, 0.012 m – were also calculated. For the outlet valley there is no in-situ information about its geology, therefore we also assume 0.005 m as a minimum possible grain size for its carving. The maximum D50 for the outlet valley is taken as 0.1 m, because outlet formation follows eastern rim breaching and could be considered as a breaching-related process and D50 = 0.1 m was already assumed for the eastern rim breaching by Salese et al., 2020.

3.3.2. *Western and Eastern rim breaching*

The breaching events of the crater rim were modeled as both catastrophic breaching and long-term erosion under constant flow scenarios. For the catastrophic breaching scenario we assume a channel width in the rim equal to the distance between the rim remnants to the north and to the south at the corresponding breaching terrace height. For example, for the 1st breaching phase of the eastern rim it is 7550 m, see Fig. 8. This follows the approach by Salese et al. (2020). For the channel depth, we modeled the range of values starting from a minimum of 5 m to a maximum possible depth for each breaching phase. The maximum possible depth is equal to the distance between the corresponding terraces; for example, for the 1st breaching phase of the eastern rim the maximum possible depth of the channel is 37 m, see Fig. 8. Intermediate values between 5 m and 190 m were included in the model with steps of 5 m. As there is no in-situ information about rim geology, we followed Salese et al., 2020 assumption of D50 = 0.1 m (cobbles), although in Fassett and Goudge (2021) they found that at D50 = 0.1 m the outlet could hardly continue to erode due to the absence of the needed positive feedback of drainage and incision. Nevertheless, there is no better estimate and therefore it can be used as an upper limit of the grain size for the rim breaching. We also added the second scenario (D50 = 0.02 m, pebbles) to check the sensitivity of the model to the grain size in the case of rim breaching.

For the long-term erosion under constant flow scenario, we assume uninterrupted long-term flow in a channel of approximately the same dimensions as the present channel in the corresponding last incised valley (for the western rim of about 190 m width and 5 m depth and for the eastern rim of about 400 m width and 13 m depth). The slopes of the channel for each breaching phase were reconstructed using slope values of the nearest rim remnants to the north and to the south from the breach. We also consider median grain sizes of 0.1 m and 0.02 m for modeling the long-term erosion under constant flow.

3.3.3. *Flooding of the crater and water outflow during breaching*

Flooding the crater up to the 1st breaching terrace (−2243 m) was modeled by only the northern inlet and by both the northern and western inlet. We did not model flooding by only the western inlet because, according to the geomorphological evidence, the northern inlet had to participate in the crater flooding before the eastern rim breaching. For the western inlet there is no such strong evidence (see Section 3.2. Geomorphological observations).

As water outflow is connected with the eastern rim erosion, we included both the median grain sizes of 0.1 m and 0.02 m in the model (the same we used for the eastern rim erosion modeling). For the channel widths and depth, we followed the methodology already described for the western and eastern rim breaching (see above). We also corrected the water outflow for water coming from both the western and northern inlets, although the effect of this correction is negligible (difference within several hours).

4. Interpretation & discussion

4.1. *Understanding of the obtained results*

Before interpreting the results, their application should be understood. In this section we call up model limitations and model assumptions to understand the meaning of the obtained results – minimum timescales and minimum water amount for each water-related event.

The model has been already validated by previous researchers using knowledge about timescales of the catastrophically formed fan in southern Iceland [Duller et al., 2008; Duller et al., 2014] and two recent river-dominated artificially originated terrestrial fan deltas: the Wax

Table 2
Timescales of water-related events.

Water-related event			Timescale (Earth years)
Northern Valley Carving		Initial valley	55–496
		Last Incised Valley	15–136
Western Valley Carving		Initial valley	407–3053
		Last Incised Valley	98–739
Outlet Valley Carving		Initial valley	1–15
		Last Incised Valley	0.4–6.2
Western Delta Deposition		Minimum extent (measured on DTM)	12.8–96.3
		Minimum extent ("tilted plane" method)	17.3–129.5
		Medium extent	24.7–185.3
		Maximum extent	54.9–412
Northern Delta Deposition		Minimum extent (measured on DTM)	7.4–67.1
		Minimum extent ("tilted plane" method)	11.7–106
		Medium extent	13.2–119.4
		Maximum extent	27.7–234.2
Western Rim Erosion	Catastrophic	D50 = 0.1	0.0014–3.7
		D50 = 0.02	0.00034–2
	Long-term	D50 = 0.1	38.5
		D50 = 0.02	20
Eastern Rim Erosion	Catastrophic	All breaching phases, D50 = 0.1	0.016–2.2
		All breaching phases, D50 = 0.02	0.00397–3.9
	Long-term	All breaching phases, D50 = 0.1	4.6–7.2
		All breaching phases, D50 = 0.02	9.3
Flooding the crater up to 1st breaching terrace		With northern inlet	6.41–6.8
		With northern and western inlets	3.19–3.4
Water outflow during breaching	Catastrophic	All breaching phases, D50 = 0.1	0.0031–0.1169
		All breaching phases, D50 = 0.02	0.0033–0.1285
	Long-term	All breaching phases, D50 = 0.1	0.35
		All breaching phases, D50 = 0.02	0.39

Lake Delta (Louisiana, USA) and the Lake Constance delta (Austria) [Salese et al., 2020]. While for the catastrophic event of a fan in southern Iceland the timescale obtained by the model of 2–17 h almost coincided with the real timescale of 6–10 h, the results for 2 recent fan deltas (the Wax Lake Delta and the Lake Constance delta) show an error by a factor of 2: the Wax Lake Delta modeled timescale is 15 years with a real time of 37 year and the Lake Constance delta modeled timescale is 50 years with a real time of 115 years. These errors may originate from the uncertainty about bank-full conditions. Appling the rule of "channel-forming discharges on Earth occur roughly for about 5% of the fluvial activity time" [Parker, 2005] (already mentioned in Section 2.1 Model description) would not help to remove the difference between the real and modeled time (for the Wax Lake Delta, 15 years / 5% = 300 years ≠ 37 years; for the Lake Constance delta, 50 years / 5% = 1000 years ≠ 115 years). Periods of intensive flooding, when rivers can even overflow the banks, also play an important role in sediment transport and decrease the timescales obtained by the model and corrected for the "5% bank-full conditions time"-rule. This apparently explains the case with the Wax Lake Delta, whose fluvial system has undergone the high flood years of 1973–1975 with abnormally high sediment flux. A similar situation is present in the Lake Constance delta fluvial system which has extreme seasonal deviations from the average ("During the peak of the thaw period in the Alps, water flow can be 10 times greater, and the amount of suspended load can increase by more than a factor of 20 times" [Salese et al., 2020]). This demonstrates the importance of the type of the water source, in this case snow melting, for water and sediment transport (ground-water sapping and precipitation influence is already described in Section 2.1. Model description). The uncertainty arising from the periodicity of the bank-full conditions, seasonal changes and also climatic changes is large on Earth, and on Mars even larger. Therefore, it can be said with confidence that timescales obtained by this model are not comparable with the real geological timescales of fluvial processes, but only show a model time of these processes based on water and sediment balances.

For the Jezero we do not know the periodicity of the bank-full conditions, and also the presence/absence and duration of dry periods with no fluvial activity are not known exactly. Salese et al., 2020 noticed that the longer the real time of formation, the more important is the role of intermittency: "if the lake formed in a catastrophic event, then intermittency is not as relevant, but if it took centuries, then it is likely that discharge fluctuated over seasonal or longer time periods". For example, for the rim erosion timescales that means, if the breaching was catastrophic, the real timescales are close to those calculated by the model. However, if breaching was by long term gradual erosion, modeled timescales would differ from the real timescales. Gradual filling with water followed by overflowing water over the rim, and again filling the resulting void, again overflowing water, etc., and also accompanied by dry periods or periods of reduced water activity with lower discharges – all these factors will result in high intermittency and increase the real timescale of the water-related events in comparison with the modeled one. Moreover, initially evaporation and water infiltration into the underground are also not included in the model. In out study, they were assessed afterwards (Section 4.3 "Calculation of the minimum available water amount). In addition, the model also is quite sensitive to some input parameters, such as slope and grain size, as shown by Salese et al., 2020.

Finally, the equilibrium erosion/bank-full flow model can underestimate the discharge of highly dynamic events like rim breaching and subsequent outlet valley carving. It is reasonable to expect that in the beginning of the valley carving the discharge at the outlet must be significantly higher than at the bank-full level, considering that initially there was no outlet channel. However, the best estimate of discharge that can be obtained within the model for the rim breaching is the bank-full discharge, which is based on the distance between the breaching terraces (see Section 3.3. Results of modeling, Western and Eastern Rim Breaching). This approach was also used by Salese et al., 2020.

Taking all the above considerations into account, timescales obtained by the model are not absolute (geological) timescales. However, they provide relative comparisons under the assumption that fluvial processes in Jezero were equally exposed to climatic factors and responded equally to their changes. This assumption is plausible as the northern inlet and western inlets were likely active at a comparable time (as shown in Scenarios 2 and 3 in Fig. 10 in Jodhpurkar et al., 2024). Therefore, the periodicity of the bank-full conditions in the western and northern inlets was the same; potential dry periods stopped activity in both inlets simultaneously and interrupted fluvial processes with the same periods of intermittency. Comparison of the timescales constraints the relative duration of the water-related events, their potential

overlapping and interconnection. Another application of the results is calculation of the minimum available amount of water as minimum provided water by inlets and minimum outflow of water through the outlet. These can be compared with each other (to draw conclusions about the balance between water input and water output) as well as with Jezero's basin volume (to check if the northern inlet could alone flood the crater). Moreover, the water amount comparison also provides a cross-check for the conclusions made during the relative comparison of the timescales. Finally, our approach provides an estimate of the total water amount Jezero crater has experienced (see next section – 4.2. Relative comparison of timescales).

4.2. Relative comparison of timescales

4.2.1. Western rim erosion and crater flooding

Here we consider a possible case when the western inlet was participating in the first crater flooding together with the northern inlet and carved the western rim on its way to the crater. Comparison of the timescales of the western rim erosion with the timescales of flooding the crater up to the 1st breaching terrace leads to different conclusions depending on the different scenarios. For a catastrophic scenario, the western rim erosion happened as fast as the flooding of the crater or faster. It means, that, when the breaching was already completed, the crater was either still being flooded or had been completely filled. For the long-term scenario it is vice versa: the western rim erosion takes much longer than flooding the crater. In this case the crater was already flooded but the western rim erosion was not still finished. It also means that eastern rim breaching could start before the western rim erosion was finished. However, there is still a possibility that the flooding of the crater started only with the western inlet, and the northern inlet joined later; the opposite situation – the beginning of flooding by the northern inlet, and the joining of the western later – is also feasible. In these cases, an estimation of the timescales is difficult and relative duration of the western rim erosion and crater flooding is unknown.

Relative comparison of timescales of the western rim erosion and crater flooding favors neither catastrophic nor long-term scenario. However, the calculation of the minimum water amount needed for western rim erosion will allow us to establish a priority scenario (Section 4.3. Calculation of the minimum available water amount).

4.2.2. Eastern rim breaching and water outflow during breaching

The timescales for the water outflow during breaching are obtained for that amount of water (236 km^3) which was stored in the crater between levels of the 1st breaching terrace (−2243 m) and the outlet floor at the rim (−2410 m). Comparison of these timescales with the timescales for the eastern rim erosion (see Table 2) shows that in most of the modeled cases in both long-term and catastrophic scenarios the eastern rim erosion lasted much longer than the water outflow. That means that 236 km^3 of water has not been enough to carve the breach. However, it is possible to find overlapping timescales for both events in the catastrophic scenario: for D50 = 0.1 the resulting (overlapping) timescales are be 0.016–0.1169 Earth years (5.84–42.67 Earth days); for D50 = 0.02 the resulting (overlapping) timescales are 0.00397–0.1285 Earth years (1.45–46.9 Earth days). These timescales are comparable with previously obtained timescales for the outlet-forming flood in Jezero (9 Earth days 20 Earth hours – see Movie S4 in Fassett and Goudge, 2021). Hence in a catastrophic scenario there is a possibility that both events – rim erosion and water outflow – happened simultaneously or, in other words, the eastern rim could have been eroded by only the 236 km^3 of water. For a long-term scenario such an overlap does not appear and in this case, a significant water supply from the inlets would be needed to finish eastern outlet rim carving.

4.2.3. Outlet valley carving and Eastern rim breaching

Comparison of the timescales obtained for the whole outlet valley carving (initial and last incised valleys together: 1.4–21.2 Earth years) with the timescales of the eastern rim erosion in *a long-term scenario* (4.6–7.23 Earth years for the grain size D50 = 0.1 and 9.32 Earth years for the grain size D50 = 0.02) shows two possibilities:

1) for the case of $0.005 < D50 < 0.02$ in the outlet valley, the timescales of the whole outlet valley carving (1.4–5.1 Earth years) are shorter than timescales for rim erosion for D50 = 0.02 (9.32 Earth years) (Table SM3). This means that the outlet carving should have been already finished while the rim erosion was still ongoing, which is impossible;
2) for D50 = 0.1 in the outlet valley, the timescales of the whole outlet valley carving (21.2 Earth years) are higher than the timescales for the rim erosion for D50 = 0.1 (4.6–7.23 Earth years). In this case rim erosion finished while outlet valley continued to carve, meaning open-basin lake conditions, which seems plausible.

In the catastrophic scenario, only in the case when breaching channel had depth 5 m and only if $D50 \leq 0.014$ m for the outlet valley, the timescale of rim erosion (3.8 Earth years) is larger than timescales for the outlet valley carving (1.4–3.7 Earth years). This again means longer rim erosion than outlet carving, which is impossible. In all other cases the outlet valley carving would last longer than rim erosion, which points to open-basin lakes condition. To sum up, most of the modeled cases, in both long-term and catastrophic scenarios, support the idea of open-basin lake conditions after eastern rim breaching.

4.2.4. Northern last incised valley carving and Northern delta deposition

Timescales for the northern last incised valley carving (15–136 Earth years) coincide with timescales of the northern delta – in the medium extent 13.2–119.4 Earth years, in minimum extent 11.7–106 Earth years and in maximum extent 27.7–234.2 Earth years. This demonstrates hydrological connectivity and consistency between these events – last valley incision and delta deposition.

4.2.5. Western last incised valley carving and Western delta deposition

Timescales for the western last incised valley carving (98–739 Earth years) overlap with the timescales obtained for the deposition of the western delta – in the maximum extent 54.9–412 Earth years, in the medium extent 24.7–185.3 Earth years, in the minimum extent 17.3–129.5. This also confirms the hydrological connectivity between the last incision of the valley and delta deposition.

4.3. Calculation of the minimum available water amount

The minimum (because it is bank-full conditions) water volume provided during initial valley carving and the last incised valley carving is calculated by multiplying the corresponding timescales by the discharges (Table 3). For each event, the minimum volume of provided/released water has a range of an order of magnitude for each event. This is explained by the range of possible scenarios we used in the model. Discharges for the last incised valley are calculated using metrics of the preserved channels within the valley (see Eq. (4)). As it is not possible to determine the discharge of the initial valleys, the same discharge as for the last incised valley was assumed (in Section 4.4 Discussion we show that increasing and decreasing of the initial valley channel sizes by a factor of 2 will not influence our interpretation). The obtained minimum volume of provided water is a multiple of the volume of Jezero's basin (See Table 3, Columns 5th and 6th). This implies the possibility of a long-term period of fluvial activity and open-lake conditions. Moreover, it also shows that the northern inlet could alone fill the crater before breaching.

The comparison of the minimum amount of water discharged during eastern rim breaching (236 km^3 was stored between the levels of the 1st breaching terrace and the outlet floor at the rim) with the water released through the outlet valley (1000–14,800 km^3) shows that the outlet valley could not have been carved only by the water stored in the crater.

Table 3
Minimum volume of water provided by inlets and released by outlet. Bank-full discharge (column 3) is calculated for the channel measured within the last incised valley.

1	2	3	4	5	6
	Timescale, Earth years	Bank-full discharge, km^3/ day	Minimum volume of provided/released water, km^3	How many times the minimum volume of water is greater than the basin volume before breaching (basin volume = 446 km^3)	How many times the minimum volume of water is greater than the basin volume after breaching (basin volume = 210 km^3)
Northern Initial Valley Carving	55–496	~0.2	3600–33,000	8–74	17–157
Northern Last Incised Valley Carving	15–136	~0.2	1000–9000	2–20	5–43
Northern Valley Total	70–632	~0.2	4600–42,000	10–94	22–200
Western Initial Valley Carving	407–3053	~0.2	27,000–203,000	60–455	128–966
Western Last Incised Valley Carving	98–739	~0.2	6500–50,000	15–112	30–238
Western Valley Total	505–3792	~0.2	33,500–253,000	75–567	158–1204
Outlet Initial Valley Carving	1–15	~1.9	700–10,500	–	–
Outlet Last Incised Valley Carving	0.4–6.2	~1.9	300–4300	–	–
Outlet Valley total	1.4–21.2	~1.9	1000–14,800	–	–

Therefore, Jezero had more water input from the inlets and consequently must have been an open-basin lake during or after eastern rim breaching. This includes the possibility of a partly-open basin, which remains closed while water is accumulating behind the weir but becomes opened as soon as water overflows. This overflow can happen as catastrophic flooding (with the discharge much higher than bank-full), or as longer overspill (with approximately bank-full discharge), or, what is most likely, the combination of both. Therefore, the real value of discharge and therefore timescale lie between these 2 extreme cases – catastrophic breaching and long-term erosion. The timescales of the most of the modeled cases for the outlet valley carving and eastern rim erosion also support the idea of the open-basin lake (see Section 4.2. Relative comparison of timescales, "*Outlet Valley Carving and Eastern Rim Erosion*"). Moreover, comparison of this amount of water of 236 km^3 with the minimum amount of water needed to carve the eastern rim breach shows the same: in most scenarios more water is needed than just 236 km^3 (see Table 4). Only in the case of the catastrophic scenario with D50 = 0.02 and channel depth = 5 m this amount of water of 236 km^3 would be sufficient to carve the breach, as only 194 km^3 would be needed (see Table 4).

Table 4
Minimum amount of water needed for rim erosion (see also detailed Calculations 1–3 in the Supplementary Materials).

Water-related event	Scenario	Median Grain Size, m	Water Volume, km^3
Western Rim Erosion	Catastrophic	0.1	924–2836
		0.02	205–1460
	Long-term	0.1	2811
		0.02	1460
Eastern Rim Erosion	Catastrophic	0.1	874–4468
		0.02	194–5158
	Long-term	0.1	3192–3781
		0.02	619

The minimum amount of water provided by inlets (38100–295,000 km^3) is higher than the minimum amount of water released out of the lake (1000–14,800 km^3). The possible explanation for this is that some water flowed through the outlet in non-bank-full conditions and parts could have been evaporated or/and drained into the underground. Taking the Jezero paleolake area as approximately 1900 km^2, the thickness of water layer which was infiltrated vary from 19 km (37,100 km^3/ 1900 km^2) to 147 km (280,200 km^3 / 1900 km^2). According to Shadab et al., 2024, infiltration capacity f_c for Noachian era for basaltic crust is 10^{-6} m/s (32 [m/year]). The infiltration of the abovementioned layer of water would last from 593 years (19 [km] / 32 [m/year]) to 4593 years (147 [km] / 32 [m/year]). These timescales of infiltration within the Jezero crater (593–4593 Earth years) are comparable with the timescales of studied events (for example, for the carving of the total western valley it is 505–3792 Earth years, see Table 2). At the same time, evaporation could also be an explanation for the substantial difference between the water volume provided by inlets and the water volume released by the outlet. However, our estimations even with the high evaporation rates (0.1–1 m/year for Eberswalde crater for present conditions – Irwin et al., 2015) give timescale of 190,000 –1,470,000 Earth years, which shows that water loss by evaporation is less significant than by infiltration.

Comparison of the minimum water volume needed for the western rim erosion (Table 4) with the water volume needed to fill the crater before breaching (446 km^3) shows that in most cases the crater flooding finished faster than western rim breaching. This is only possible in the long-term scenario (see Section 4.2. Relative comparison of timescales). This comparison could also explain why there are no terraces in the western inlet which would lie at the same heights as terraces at the eastern outlet rim. In most of the modeled cases the western rim would not have been carved down to these levels when the eastern rim breaching started to happen. At the same time this conclusion confirms our assumption, that the northern rim was already eroded by the time of the northern inlet activity (see Section 3.1. Results of measurements). If not, there would have been the same situation as in the western inlet and

we would not find any terraces at the same levels as the breaching terraces in the outlet on the eastern rim.

If the first crater flooding was a continuous process and was not interrupted by dry periods, enough water to flood the crater and cause the eastern rim breaching would be provided already during the first stages of the initial valley carving. Therefore, most of the volume of the valleys was eroded already after the eastern rim was breached.

4.4. Discussion

4.4.1. Missing sediments and the fresh crater case

If sediments from the last incision of the valleys were deposited in the northern and western deltas (Sections 3.1. Results of measurements and Section 3.3 Results of modeling), the question arises: Where are the ~43 km^3 of sediments eroded from the initial valleys and the western rim breach? One possible explanation could be an interruption of fluvial activity and complete drying of the Jezero lake before the resumption of activity. During such an intermittency extensive wind erosion could occur, blowing away the missing sediments. The significant exhumation of the whole region and missing material around Jezero is also reported by Bamber et al., 2022.

Another possibility is that basalt emplacement could bury the older sediments transported from the initial valleys and western rim breach. The rough estimation of the volume of the last visible basalt layer, which underlies the present delta ([Russell et al., 2023], [Paige et al., 2024]) gives a value of ~11 km^3 derived by multiplication of the volcanic unit maximum thickness of ~30 m [Schon et al., 2012] by its area of ~350 km^2. There could have been more basalt layers underneath. In the extreme case, sediments from the initial valleys were eroded and transported to the crater floor when the crater was still fresh without any infilling. To estimate the volume of the fresh crater we integrated a function describing the fresh crater profile from the center point to the rim, which was obtained using the empirical formulas from Kleinhans et al., 2010 and Garvin and Frawley, 2003 (see also Supplementary Material, Calculations 4–6). Calculation of the volume of the fresh crater is based on its diameter. The diameter measurement yield uncertain results because the crater rim is partly eroded and it is difficult to find the crest line on the crater rim. In our study we obtained the value of 50 km for diameter (the same as in [Stack et al., 2020], [Salese et al., 2020]) using the 3 highest points on the rim to reconstruct the rim crest. However, also values of 45 km [Mangold et al., 2021] and 47.52 km [Gazetteer of Planetary Nomenclature, International Astronomical Union (IAU), 2024] were obtained by previous researchers. We calculated crater volumes for these diameters to show the sensitivity of this method to the diameter (Table 5): increasing the diameter by 5 km (~11 %, from 45 km to 50 km) will increase the volume by 473 km^3 (~31 %, from 1549 to 2022 km^3) which makes a considerable difference. Table 5 shows that ~43 km^3 of sediments missing from the initial valleys and western rim breach can easily be a part of the crater infilling which yields approximately 1100–1580 km^3 (calculated as the difference between the fresh and the present crater volume).

Another question arises in connection with the fresh crater case: could the northern inlet alone flood the crater during the initial valley carving? For that, it had to fill the 2022 km^3 of the fresh crater with water, which is still less than the 3600–33,000 km^3 of water provided during the initial valley incision (Table 3). However, the timescales for the northern initial valley carving were estimated based on the assumption that the initial valley contained the same channel with the same dimensions as the last incised valley do (Section 3.3. Results of modeling, *"Valleys Carving and Delta Depositions"*). But even if the real channel in the initial valley was 2 times larger or smaller than assumed in this study, the northern inlet alone could still flood the fresh crater completely (Supplementary Material, Calculation 7). In addition, the water volume calculated here is still a minimum value, as we consider only bank-full conditions. In non-bank-full conditions, even more water would be provided, leaving no doubt about the possibility of flooding the fresh crater by the northern inlet alone.

Table 5
Jezero fresh crater volume estimations.

Diameter (km)	Fresh crater volume (km^3)	Infilling volume in the present crater (km^3)
45	1549	1103
47.52	1778	1332
50	2022	1576

4.4.2. Comparison with previous studies

The evolution of the Jezero basin started with the flooding of the crater. In our study we showed that it was not done only by the western inlet, as previously thought (Salese et al., 2020), but either by the northern inlet alone or by the northern and western inlets together. The evidence for this is terraces in the northern inlet at the same heights as breaching terraces at the eastern rim breach. For the first time we also considered the western rim erosion which had to happen during the crater flooding. Most of the modeled cases show that the western rim erosion lasts longer than the crater flooding. We also showed that the northern rim was already eroded by the time of the fluvial activity, as indicated by the morphological comparison with the western rim and calculations of the minimum provided water (see Section 4.3. Calculation of the minimum available water amount).

The second stage of evolution is breaching of the eastern rim in at least 3 episodes which were found by Salese et al., 2020. We add to this that at that point, when the eastern rim erosion started, the western rim breaching was not yet completed (in most of the modeled cases, >95 %). We also found out that the amount of water stored in the crater between the levels of the 1st breaching terrace and the outlet floor at the eastern rim was not enough to erode the eastern rim breach and outlet valley. This implies that Jezero was an open-basin lake during or after the eastern rim breaching. These results are in agreement with previous studies [Fassett and Head, 2005], [Schon et al., 2012], [Goudge et al., 2015], etc. At the end of the eastern rim breaching stage, most of the last valley incision occurred and most of the volume of the northern and western deltas was deposited. The explanation for this is that both northern and western delta lie a little bit higher than the outlet floor at the eastern rim, implying that they started to deposit material already during the 3rd phase of the eastern rim breaching.

Finally, the lake level drops as soon as the water balance is negative. After a complete stop of the water supply it dries out/seeps out and disappears. In our study we also introduced the possibility of several events of drying and flooding, because such an intermittency in fluvial activity could explain the absence of the ~43 km^3 of sediments carved from the initial valleys and the western rim. For this, the lake must have dried out at least once before the deposition of the present deltas, allowing wind erosion to blow away the sediments or deposition of basalts to cover them.

There is still a discussion if the eastern rim breaching as well as the western rim breaching, which was never studied in detail before and still raises questions (for example, the western inlet formation mechanism and its relationship with rim erosion is unknown – [Bamber et al., 2022]), formed in catastrophic events or by long carving with multiple overflow events. In Salese et al., 2020 there is no final answer to this question: "…it had at least three catastrophic collapses or it overflowed for a long (unknown) time such that it carved out the breach". Other researchers tend to have different points of view. The maturity of the outlet channel, according to Schon et al., 2012, suggests the breaching in a non-catastrophic manner. The 1D model of Fassett and Goudge, 2017 implied slow fluvial erosion (over tens of thousands of years), while 2D model (in BASEMENT) was consistent with catastrophic carving of the outlet under a narrow set of assumptions. Holo and Kite's, 2017 results show that the observed incised depth of the outlet can be obtained

within ~100 years after the onset of sediment transport. Goudge et al., 2019 studied 24 basins (including Jezero) and found a correlation between total drained volume and Martian paleolake geometry. In the Jezero case this correlation supports that the outlet incision was the result of a single lake overflow flood, although they also considered multiple flooding events and incision by longer-term overflow. Finally, the model of Fassett and Goudge, 2021 suggest that for large lakes like Jezero a single catastrophic flood is sufficient for outlet incision. Each model has its limitations – hydrodynamic and sediment transport assumptions, boundary conditions uncertainties, accuracy of the data, etc. In addition, the mechanism of the crater rim breaching on Mars – overtopping, piping or induced slumping [Fassett and Goudge, 2021] – is also unknown. In our study we assumed an overtopping mechanism and modeled both catastrophic and long-term scenarios although for the long-term erosion still without possible intermittency between the short overflowing events. We found that the long-term scenario is the most probable for the western rim breaching, which lasted longer than the crater flooding. And for the eastern rim, the results of modeling do not prioritize any one scenario but show that in both the long-term and catastrophic scenarios breaching lasted much longer than the outflow of water stored in the crater before breaching.

5. Conclusions

In our study:

1) The water-related processes in the Jezero crater were modeled, including events which have not previously been fully or extensively studied: western rim erosion, flooding of the crater by only the northern inlet and by both the northern and the western inlet, northern delta deposition.
2) Other processes which were studied before by other researchers – western valley carving, western delta deposition, eastern rim erosion and water outflow during breaching – were remodeled using a wider range of scenarios and our new measurements. For valley carving and delta deposition we incorporated findings from the Perseverance rover; for rim breaching we modeled both catastrophic and long-term scenarios.
3) Detailed geomorphological observations allowed us to identify: a) two stages of valley carving each of the inlets and the outlet; b) the presence of the terraces in the northern inlet (which strongly coincide with the height of the breaching terraces at the eastern outlet rim); c) the absence of such terraces in the western inlet, and d) the height position of the deltas relative to the outlet floor at the eastern rim.
4) Detailed mapping of the two stages of valley carving (initial valley and last incised valley) as well as delta mapping in 3 extents (minimum, medium and maximum) provided us the base for the geomorphic measurements.
5) Uncertainties of the used model are also carefully investigated to identify the limitations and put the interpretation on a stable basis.
6) The obtained timescales of the model constrain the available water for each water-related event within the Jezero crater.
7) The location of the missing sediments from the initial valleys and western rim breach was discussed with the possibility of the fresh crater flooding.
8) Our results and interpretations support and improve previous studies.

The conclusions of our study are presented in Table 6 (the most important conclusions are in bold). We show that the history, order and relative duration of the water-related processes in the Jezero crater could be more complicated than previously thought. We proved that the northern inlet was involved in the first crater flooding and subsequent eastern rim breaching. The inlets as well as the outlet had at least 2 incision events, and deltas were deposited during the last incision event.

Table 6
Conclusions and explanations (the most important conclusions are in bold).

№	Conclusion	Explanation
1	**The northern inlet participated in the first crater flooding and the eastern rim breaching.**	Inlet has terraces at the same heights as the breaching terraces of the outlet.
2	**The northern inlet alone could have flooded the crater.**	The minimum volume of water provided during the northern valley carving exceeds the volume needed to fill the crater before breaching (even if it was a fresh crater without any infilling).
3	The western inlet probably also participated in the first crater flooding.	The western valley is more developed than the northern valley, therefore it could have been also active during the northern inlet activity.
4	The western rim erosion lasts longer than the crater flooding; the eastern rim breaching started before the western rim erosion was finished (if the western inlet participated in the first crater flooding).	The minimum water volume needed for the western rim erosion is larger than the water volume needed to fill the crater before breaching (446 km^3) – in most of the modeled cases (>95 %).
5	The western inlet does not show terraces at the same heights as the breaching terraces in the outlet because the western rim was most likely not carved down to these levels at the time of the eastern rim breaching (if the western inlet participated in the first crater flooding).	Result of the most of the modeled cases (>95 %) – see above conclusion №4
6	The northern rim was already eroded by the time of fluvial activity.	If not, the northern inlet would not contain terraces at the breaching heights (as the western inlet now, №4) because it would not most likely be carved down to the levels of the breaching phases.
7	Most of the volume of the valleys was eroded already after the eastern rim breaching (if the crater flooding was a continuous process).	The necessary amount of water to flood the crater and cause the eastern rim breaching was already provided during the first stages of the initial valley carving.
8	The eastern rim breaching lasted longer than the water outflow (outflow of 236 km^3 of water, stored between the levels of the 1st breaching terrace and the outlet floor at the rim).	Showed by most of the modeled cases (>90 %) in both long-term and catastrophic scenarios.
9	**Jezero was an open-basin lake during or after the eastern rim breaching.**	1) The water volume stored between the levels of the 1st breaching terrace and the outlet floor at the rim (236 km^3) is lower than the minimum amount of water which flowed through the outlet valley – in all modeled cases. 2) The water volume stored between the levels of the 1st breaching terrace and the outlet floor at the rim (236 km^3) is lower than the minimum amount of water needed to carve the eastern rim breach – in most of the modeled cases (>90 %). 3) The timescales for the outlet valley carving are longer than for the eastern rim erosion – in most of the modeled cases (>90 %).
10	**The northern and western deltas were deposited during the last**	The amount of the sediments carved from valleys almost coincides with the amount of the sediments

(*continued on next page*)

Table 6 (*continued*)

N°	Conclusion	Explanation
	incisions of the corresponding inlets.	deposited in the corresponding deltas; the same for the timescales of the valley carving and delta deposition.
11	The deltas were deposited after the eastern rim breaching, not earlier than the 3rd breaching phase (under the assumption that they were not much higher in the past than currently).	Both deltas lie below −2360 m – the level of the water within the 3rd breaching phase of the eastern rim.
12	The last incisions of the inlet valleys happened not earlier than the 3rd breaching phase of the eastern rim.	Because the last incision of the valleys is connected to the deposition of the deltas (see conclusion N°10), and the deltas lie below −2360 m – the level of water within the 3rd breaching phase (see conclusion N°11).

Finally, each inlet, even separately, could provide enough water to flood the crater multiple times and maintain an open-basin lake within the crater. Our findings, although do not completely reconstruct the past of the Jezero paleolake in geological times, but still shed light on the fluvial and sediment transport processes and condition of the water history in Jezero.

CRediT authorship contribution statement

Anastasiia Ovchinnikova: Writing – original draft, Visualization, Methodology, Investigation, Conceptualization. **Ralf Jaumann:** Writing – original draft, Supervision, Investigation, Conceptualization. **Sebastian H.G. Walter:** Writing – review & editing, Software. **Christoph Gross:** Writing – review & editing, Validation. **Wilhelm Zuschneid:** Writing – review & editing, Validation. **Frank Postberg:** Writing – review & editing, Resources, Project administration.

Declaration of competing interest

The authors declare that they have no known competing financial interests or personal relationships that could have appeared to influence the work reported in this paper.

Data availability

The CTX and HiRISE data are available through the Planetary Data System Imaging Node at https://pds-imaging.jpl.nasa.gov/. The HRSC terrain models and image data are available at the data archives of ESA and NASA and in the map-based data portal at https://maps.planet.fu-berlin.de (Walter et al., 2018).The dataset with the shape-files of the mapped valleys and deltas in the Jezero crater is available at https://doi.org/10.17169/refubium-45033 (Ovchinnikova and Jaumann, 2024).

Acknowledgements

We thank the HRSC experiment teams at DLR and ESA, and the HiRISE and CTX operations and science teams at JPL and ASU. We also thank Fred Calef for personal communication about his dataset “Mars 2020 Science Investigation CTX DEM Mosaic”. This work is partially supported by the German Space Agency (DLR Bonn), Grant 50 OO 2204, on behalf of the German Federal Ministry for Economic Affairs and Climate Action. This research has made use of the USGS Integrated Software for Imagers and Spectrometers (ISIS). Open Access funding enabled and organized by Projekt DEAL.

We also thank the reviewers Caleb Fassett and Ben Cardenas for their detailed and insightful comments which helped us to improve the manuscript.

Appendix A. Supplementary data

Supplementary data to this article can be found online at https://doi.org/10.1016/j.icarus.2024.116349.

References

Adeli, S., Hauber, E., Kleinhans, M., Le Deit, L., Platz, T., Fawdon, P., Jaumann, R., 2016. Amazonian-aged fluvial system and associated ice-related features in Terra Cimmeria, Mars. Icarus 277, 286–299. https://doi.org/10.1016/j.icarus.2016.05.020.

Annex, A.M., Ehlmann, B.L., 2024. Elevation anomalies of the volcanic floor unit and their relationships to the multiple Lakes of Jezero crater, Mars. Geophys. Res. Lett. 51 (6). https://doi.org/10.1029/2023GL108069.

Bamber, E.R., Goudge, T.A., Fassett, C.I., Osinski, G.R., 2022. Constraining the formation of paleolake inlet valleys across crater rims. Icarus 378. https://doi.org/10.1016/j.icarus.2022.114945.

Baum, M., Wordsworth, R., Goudge, T.A., 2021. Consequences of proposed shoreline deformation scenarios for jezero crater, mars. Planet. Sci. J. 2 (4). https://doi.org/10.3847/PSJ/ac01de.

Beyssac, et al., 2024. What are the olivine-rich boulders in the upper fan and margin unit at Jezero crater, Mars?. In: 55th Lunar and Planetary Science Conference 3040.

Bibring, J.P., et al., 2006. Global mineralogical and aqueous Mars history derived from OMEGA/Mars express data. Science 312 (5772), 400–404. https://doi.org/10.1126/science.1122659.

Buhler, P.B., Fassett, C.I., Head, J.W., Lamb, M.P., 2014. Timescales of fluvial activity and intermittency in Milna crater, Mars. Icarus 241, 130–147. https://doi.org/10.1016/j.icarus.2014.06.028.

Butcher, F.E.G., Conway, S.J., Arnold, N.S., 2016. Are the dorsa Argentea on Mars eskers? Icarus 275, 65–84. https://doi.org/10.1016/j.icarus.2016.03.028.

Butcher, F.E.G., et al., 2020. Morphometry of a glacier-linked esker in NW Tempe Terra, Mars, and implications for sediment-discharge dynamics of subglacial drainage. Earth Planet. Sci. Lett. 542. https://doi.org/10.1016/j.epsl.2020.116325.

Calef, F., 2021. Mars 2020 Science Investigation CTX DEM Mosaic [Dataset], Planetary Data System. USGS Astrogeology Science Center. https://astrogeology.usgs.gov/search/map/mars_2020_science_investigation_ctx_dem_mosaic.

Chau, T.K., Toan, N.T., Duc, D.A., Linh, N.H., 2021. Developing the regression equations to determine the Bank-full discharge from the basin characteristics. Arch. Hydroeng. Environ. Mech. 68 (2), 103–117. https://doi.org/10.2478/heem-2021-0006.

Comer, R.P., Solomon, S.C., Head, J.W., 1985. Mars: thickness of the lithosphere from the tectonic response to volcanic loads. Rev. Geophys. https://doi.org/10.1029/RG023i001p00061.

Corpolongo, A., et al., 2023. SHERLOC Raman mineral class detections of the Mars 2020 crater floor campaign. J. Geophys. Res. Planets 128 (3). https://doi.org/10.1029/2022JE007455.

Coulson, I.M., Beech, M., Nie, W., 2007. Physical properties of Martian meteorites: porosity and density measurements. Meteorit. Planet. Sci. 42 (12), 2043–2054. https://doi.org/10.1111/j.1945-5100.2007.tb01006.x.

Duller, R.A., Mountney, N.P., Russell, A.J., Cassidy, N.C., 2008. Architectural analysis of a volcaniclastic jökulhlaup deposit, southern Iceland: sedimentary evidence for super critical flow. Sedimentology 55 (4), 939–964. https://doi.org/10.1111/j.1365-3091.2007.00931.x.

Duller, R.A., Warner, N.H., McGonigle, C., De Angelis, S., Russell, A.J., Mountney, N.P., 2014. Landscape reaction, response, and recovery following the catastrophic 1918 Katla jökulhlaup, southern Iceland. Geophys. Res. Lett. 41 (12), 4214–4221. https://doi.org/10.1002/2014GL060090.

Dunne, T., 1990. Hydrology, mechanics, and geomorphic implications of erosion by subsurface flow. Groundwater morphology: the role of subsurface water in earth-surface processes and landforms. Spec. Pap. Geol. Soc. Am. 252, 1–28.

Ehlmann, B.L., et al., 2008. Clay minerals in delta deposits and organic preservation potential on Mars. Nat. Geosci. 1 (6), 355–358. https://doi.org/10.1038/ngeo207.

Engelund, F., Hansen, E., 1967. A Monograph on Sediment Transport in Alluvial Streams. Teknisk Forlag, Kobenhavn, Denmark.

Farley, K.A., et al., 2022. Aqueously altered igneous rocks sampled on the floor of Jezero crater, Mars. Science 377 (6614). https://doi.org/10.1126/science.abo2196.

Fassett, C.I., Goudge, T.A., 2017. Hydrological Modeling of the Jezero Crater Outlet-Forming Flood. Lunar and Planetary Science XLVIII.

Fassett, C.I., Goudge, T.A., 2021. Modeling the hydrodynamics, sediment transport, and valley incision of outlet-forming floods from Martian Crater Lakes. J. Geophys. Res. Planets 126 (11). https://doi.org/10.1029/2021JE006979.

Fassett, C.I., Head, J.W., 2005. Fluvial sedimentary deposits on Mars: ancient deltas in a crater lake in the Nili fossae region. Geophys. Res. Lett. 32 (14), 1–5. https://doi.org/10.1029/2005GL023456.

Fassett, C.I., Head, J.W., 2008. The timing of Martian valley network activity: constraints from buffered crater counting. Icarus 195, 61–89. https://doi.org/10.1016/j.icarus.2007.12.009.

Fergason, R.L., et al., 2020. Mars 2020 terrain relative navigation product generation: digital model and orthorectified image mosaics. In: 51st Annual Lunar and Planetary Science Conference.

Garvin, J.B., Frawley, J.J., 2003. Craters on Mars: global geometric properties from gridded MOLA topography. In: Sixth International Conference on Mars, 2003, pp. 7–9.
Gazetteer of Planetary Nomenclature, International Astronomical Union (IAU), 2024. https://planetarynames.wr.usgs.gov/Feature/14300.
Goudge, T.A., Mustard, J.F., Head, J.F., Fassett, J.W., Russel, J.M., 2013. Assessing Catchment and delta Mineralogy within the Jezero Crater Paleolake System: A Combined Mapping and Terrestrial Analog Approach (GSA Annual Meeting in Denver).
Goudge, T.A., Mustard, J.F., Head, J.W., Fassett, C.I., Wiseman, S.M., 2015. Assessing the mineralogy of the watershed and fan deposits of the Jezero crater paleolake system, Mars. J. Geophys. Res. Planets 120 (4), 775–808. https://doi.org/10.1002/2014JE004782.
Goudge, T.A., Mohrig, D., Cardenas, B.T., Hughes, C.M., Fassett, C.I., 2018. Stratigraphy and paleohydrology of delta channel deposits, Jezero crater, Mars. Icarus 301, 58–75. https://doi.org/10.1016/j.icarus.2017.09.034.
Goudge, T.A., Fassett, C.I., Mohrig, D., 2019. Incision of paleolake outlet canyons on Mars from overflow flooding. Geology 47 (1), 7–10. https://doi.org/10.1130/G45397.1.
Gwinner, K., Scholten, F., Spiegel, M., Schmidt, R., Giese, B., Oberst, J., Heipke, C., Jaumann, R., Neukum, G., 2009. Derivation and validation of high-resolution digital terrain models from mars express HRSC data. Photogramm. Eng. Remote. Sens. 75 (9), 1127–1142. https://doi.org/10.14358/PERS.75.9.1127.
Gwinner, K., et al., 2016. The high resolution stereo camera (HRSC) of Mars express and its approach to science analysis and mapping for Mars and its satellites. Planet. Space Sci. 126, 93–138. https://doi.org/10.1016/j.pss.2016.02.014.
Harvey, A.M., 1969. Channel capacity and the adjustment of streams to hydrologic regime. J. Hydrol. 8 (1), 82–98. https://doi.org/10.1016/0022-1694(69)90032-8.
Hiesinger, H., Head, J.W., 2004. The syrtis major volcanic province, Mars: synthesis from Mars global surveyor data. J. Geophys. Res. Planets 109 (1). https://doi.org/10.1029/2003je002143.
Hoke, M.R.T., Hynek, B.M., Tucker, G.E., 2011. Formation timescales of large Martian valley networks. Earth Planet. Sci. Lett. 312 (1–2), 1–12. https://doi.org/10.1016/j.epsl.2011.09.053.
Holm-Alwmark, S., et al., 2021. Stratigraphic relationships in Jezero crater, Mars: constraints on the timing of fluvial-lacustrine activity from orbital observations. J. Geophys. Res. Planets 126 (7). https://doi.org/10.1029/2021JE006840.
Holo, S., Kite, E.S., 2017. Incision of the Jezero Crater outflow channel by fluvial sediment transport. In: American Geophysical Union, Fall Meeting 2017, Abstract #EP41B-1837.
Horvath, D.G., Andrews-Hanna, J.C., 2024. The hydrology of the Jezero crater paleolake: implications for the climate and limnology of the lake system from hydrological modeling. Earth Planet. Sci. Lett. 635. https://doi.org/10.1016/j.epsl.2024.118690.
Howard, A.D., Craig Kochel, R., Holt, H.E., 1988. Sapping features of the Colorado plateau: a comparative planetary geology field guide. Natl. Aeronaut.Space Administr. 1–108.
Irwin, R.P., Lewis, K.W., Howard, A.D., Grant, J.A., 2015. Paleohydrology of Eberswalde crater, Mars. Geomorphology 240, 83–101. https://doi.org/10.1016/j.geomorph.2014.10.012.
Ivanov, M.A., Hiesinger, H., Erkeling, G., Hielscher, F.J., Reiss, D., 2012. Major episodes of geologic history of Isidis Planitia on Mars. Icarus 218 (1), 24–46. https://doi.org/10.1016/j.icarus.2011.11.029.
Jaumann, R., Nass, A., Tirsch, D., Reiss, D., Neukum, G., 2010. The Western Libya Montes Valley system on Mars: evidence for episodic and multi-genetic erosion events during the Martian history. Earth Planet. Sci. Lett. 294, 272–290. https://doi.org/10.1016/j.epsl.2009.09.026.
Jaumann, R., et al., 2014. Water and Martian habitability: results of an integrative study of water related processes on Mars in context with an interdisciplinary Helmholtz research alliance “planetary Evolution and Life.”. Planet. Space Sci. 98, 128–145. https://doi.org/10.1016/j.pss.2014.02.013.
Jodhpurkar, M., Bell, J., 2024. Northern fan deposits in Jezero crater, Mars [dataset]. Mendeley Data V1. https://doi.org/10.17632/mph7pj2sjc.1.
Jodhpurkar, M.J., et al., 2024. Mapping and characterizing the northern fan deposits in Jezero crater, Mars. J. Geophys. Res. Planets 129. https://doi.org/10.1029/2024JE008308.
Kleinhans, M.G., 2005. Flow discharge and sediment transport models for estimating a minimum timescale of hydrological activity and channel and delta formation on Mars. J. Geophys. Res. Planets 110 (12), 1–23. https://doi.org/10.1029/2005JE002521.
Kleinhans, M.G., van Rijn, L.C., 2002. Stochastic prediction of sediment transport in sand-gravel bed Rivers. J. Hydraul. Eng. 128 (4), 412–425. https://doi.org/10.1061/(asce)0733-9429(2002)128:4(412).
Kleinhans, M.G., van de Kasteele, H.E., Hauber, E., 2010. Palaeoflow reconstruction from fan delta morphology on Mars. Earth Planet. Sci. Lett. 294 (3–4), 378–392. https://doi.org/10.1016/j.epsl.2009.11.025.
Laity, J.E., Malin, M.C., 1985. Sapping processes and the development of theater-headed valley networks on the Colorado plateau. Geol. Soc. Am. Bull. 96 (2), 203–217. https://doi.org/10.1130/0016-7606(1985)96<203:SPATDO>2.0.CO;2.
Leopold, L.B., Wolman, M.G., Miller, J.P., 1964. Fluvial Processes in Geomorphology. W. H. Freeman and Company, San Francisco. https://doi.org/10.2307/213147.
Malin, M.C., et al., 2007. Context camera investigation on board the Mars reconnaissance orbiter. J. Geophys. Res. Planets 112 (5). https://doi.org/10.1029/2006JE002808.
Mangold, N., et al., 2007. Mineralogy of the Nili fossae region with OMEGA/Mars express data: 2. Aqueous alteration of the crust. J. Geophys. Res. Planets 112 (8). https://doi.org/10.1029/2006JE002835.
Mangold, N., et al., 2012. The origin and timing of fluvial activity at Eberswalde crater, Mars. Icarus 220 (2), 530–551. https://doi.org/10.1016/j.icarus.2012.05.026.
Mangold, N., et al., 2020. Fluvial regimes, morphometry, and age of Jezero crater Paleolake inlet valleys and their exobiological significance for the 2020 rover Mission landing site. Astrobiology 20 (8), 994–1013. https://doi.org/10.1089/ast.2019.2132.
Mangold, N., et al., 2021. Perseverance rover reveals an ancient delta-lake system and flood deposits at Jezero crater, Mars. Science 374 (6568). https://doi.org/10.1126/science.abl4051.
Mangold, N., et al., 2024. Past variations of water level of Jezero paleolake. In: 55th Lunar and Planetary Science Conference.
Meyer-Peter, E., Mueller, R., 1948. Formulas for bed-load transport. In: Proceedings 2nd Meeting, International Symposium on Hydraulic Structures Research, Stockholm, pp. 39–64.
Michalski, J.R., Goudge, T.A., Crowe, S.A., Cuadros, J., Mustard, J.F., Johnson, S.S., 2022. Geological diversity and microbiological potential of lakes on Mars. Nat. Astron. Nat. Res. https://doi.org/10.1038/s41550-022-01743-7.
Mottl, M.J., Glazer, B.T., Kaiser, R.I., Meech, K.J., 2007. Water and astrobiology. Chem. Erde 67 (4), 253–282. https://doi.org/10.1016/j.chemer.2007.09.002.
Murchie, S.L., et al., 2009. A synthesis of Martian aqueous mineralogy after 1 Mars year of observations from the Mars reconnaissance orbiter. J. Geophys. Res. Planets 114 (9). https://doi.org/10.1029/2009JE003342.
Ovchinnikova, A., Jaumann, R., 2024. Valleys and deltas in Jezero crater, Mars [Dataset]. Refubium. doi:10.17169/refubium-45033.
Paige, D.A., et al., 2024. Ground penetrating radar observations of the contact between the western delta and the crater floor of Jezero crater, Mars. Sci. Adv. 10 (4). https://doi.org/10.1126/sciadv.adi83.
Parker, G., 2005. Chap. 3, Transport of gravel and sediment mixtures. In: Sedimentation Engineering, ASCE Manual 54, vol. 2. American Society of Civil Engineering, New York, p. 131.
Poulet, F., et al., 2005. Phyllosilicates on Mars and implications for early martian climate. Nature 438 (7068), 623–627. https://doi.org/10.1038/nature04274.
Rice, M.S., et al., 2023. Spectral variability of rocks and soils on the Jezero crater floor: a summary of multispectral observations from Perseverance’s Mastcam-Z instrument. J. Geophys. Res. Planets 128 (10). https://doi.org/10.1029/2022JE007548.
Robbins, S.J., Hynek, B.M., Lillis, R.J., Bottke, W.F., 2013. Large impact crater histories of Mars: the effect of different model crater age techniques. Icarus 225 (1), 173–184. https://doi.org/10.1016/j.icarus.2013.03.019.
Russell, P.S., et al., 2023. Stratigraphy relationships of the Delta and crater floor in Jezero crater from RIMFAX GPR observations. In: 54th Lunar and Planetary Science Conference.
Salese, F., Kleinhans, M.G., Mangold, N., Ansan, V., McMahon, W., De Haas, T., Dromart, G., 2020. Estimated minimum life span of the Jezero Fluvial Delta (Mars). Astrobiology 20 (8), 977–993. https://doi.org/10.1089/ast.2020.2228.
Schon, S.C., Head, J.W., Fassett, C.I., 2012. An overfilled lacustrine system and progradational delta in Jezero crater, Mars: implications for Noachian climate. Planet. Space Sci. 67 (1), 28–45. https://doi.org/10.1016/j.pss.2012.02.003.
Shadab, M.A., Hiatt, E., Bahia, R.S., Bohacek, E.V., Steinmann, V., Hesse, M.A., 2024. Infiltration on early Mars and its implication towards fluvial-Aeolian interactions. In: 55th Lunar and Planetary Science Conference 3040.
Sharma, S., et al., 2023. Diverse organic-mineral associations in Jezero crater, Mars. Nature 619 (7971), 724–732. https://doi.org/10.1038/s41586-023-06143-z.
Silberman, E., Carter, R., Einstein, H., Hinds, J., Powell, R., ASCE Task Force on Friction Factors in Open Channels, 1963. Friction factors in open channels. J. Hydraul. Eng. 89 (HY2), 97–143.
Simon, A., Dickerson, W., Heins, A., 2004. Suspended-sediment transport rates at the 1.5-year recurrence interval for ecoregions of the United States: transport conditions at the bank-full and effective discharge? Geomorphology 58 (1–4), 243–262. https://doi.org/10.1016/j.geomorph.2003.07.003.
Stack, K.M., et al., 2020. Photogeologic Map of the Perseverance Rover Field Site in Jezero Crater Constructed by the Mars 2020 Science Team. Space Science Reviews. Springer Science and Business Media B.V. https://doi.org/10.1007/s11214-020-00739-x.
Stack, K.M., et al., 2024. Sedimentology and stratigraphy of the Shenandoah formation, Western fan, Jezero crater, Mars. J. Geophys. Res. Planets 129 (2). https://doi.org/10.1029/2023JE008187.
Tanaka, K.L., et al., 2014. Geologic Map of Mars: U.S. Geological Survey Scientific Investigations Map 3292, Scale 1:20,000,000, Pamphlet, p. 43. https://doi.org/10.3133/sim3292.
Walter, S.H.G., et al., 2018. The web-based interactive Mars analysis and research system for HRSC and the iMars project. Earth Space Sci. 5, 308–323. https://doi.org/10.1029/2018EA000389.
Wichman, R.W., Schultz, P.H., 1989. Sequence and mechanisms of deformation around the Hellas and Isidis impact basins on Mars. J. Geophys. Res. 94 (B12). https://doi.org/10.1029/jb094ib12p17333.